MICROCOPY RESOLUTION TEST CHART

NATIONAL BUREAU OF STANDARDS 1963 A

LEVEL

**DEFENCE RESEARCH ESTABLISHMENT
ATLANTIC**

DTIC
SELECTED
DEC 2 1980
C

A STUDY OF FILLED AND SPARSE
LINE ARRAY BEAMFORMERS

D.R.E.A. TECHNICAL MEMORANDUM 80/G

RESEARCH AND DEVELOPMENT BRANCH
DEPARTMENT OF NATIONAL DEFENCE
CANADA

DEFENCE RESEARCH ESTABLISHMENT ATLANTIC

DARTMOUTH N.S.

D.R.E.A. TECHNICAL MEMORANDUM 80/G

A STUDY OF FILLED AND SPARSE LINE ARRAY BEAMFORMERS

R. S. Walker

September 1980

Approved by   R. F. Brown   Director / Underwater Acoustics Division

DISTRIBUTION APPROVED BY

CHIEF D. R. E. A.

RESEARCH AND DEVELOPMENT BRANCH
DEPARTMENT OF NATIONAL DEFENCE
CANADA

i

ABSTRACT

The paper considers various methods of frequency-domain beamforming for a line array of hydrophones. The line array geometries are restricted to uniform sensor spacings (i.e. filled array) or a geometry in which sensors are eliminated from the filled structure (sparse array). The methods to be examined include the conventional phase-to-plane beamformer (CB), the data-adaptive Minimum Variance beamformer (MVB), and the Principal-Solution beam-former (PSB). The beamformer performance is assessed on the basis of two criteria. The first is the ability of the beamformer to map the direction-ality of the acoustic field. The integration time used in producing the map is unrestricted; hence, only first-order beamformer statistics influence the performance. The second criterion is the ability to detect narrowband, direc-tional signals against the noise. Here the integration time is finite, and higher-order beamformer statistics become important. We shall show that the PSB has advantages over the CB for mapping of the directionality. However, no advantage exists in the signal detection application. The MVB provides the directionality map that is least influenced by leakage. However, its detection performance is superior to that of the CB only if the noise field is highly directional.

ii

RÉSUMÉ

L'auteur étudie diverses méthodes d'analyse par transformées de la fréquence, utilisées pour former le faisceau de réponse acoustique d'un réseau d'hydrophones disposés en ligne. Les deux seuls réseaux linéaires possibles sont le réseau à espacement uniforme entre capteurs (c'est-à-dire le réseau plein) et le réseau dans lequel un certain nombre de capteurs sont éliminés (réseau épars). Les méthodes examinées comprennent le formateur de faisceau phase-plan classique (CB), le formateur de faisceau à variance minimale et à adaptation des données (MVB) et le formateur de faisceau à solution principale (PSB). Deux critères servent à évaluer la performance du formateur de faisceau. Le premier est l'aptitude du formateur de faisceau à produire un diagramme de directivité du champ acoustique. Aucune restriction n'est apportée au temps d'intégration nécessaire pour produire le diagramme; par conséquent, seules les données statistiques du premier ordre influent sur la performance. Le deuxième critère est l'aptitude à détecter dans le bruit ambiant les signaux directifs à bande étroite. Dans ce cas, le temps d'intégration est fini et les données statistiques d'ordre élevé deviennent importantes. L'auteur démontre que le PSB possède des avantages par rapport au CB pour produire le diagramme de directivité. Toutefois, il ne comporte aucun avantage en ce qui concerne la détéction des signaux. Le MVB produit le diagramme de directivité qui est le moins influencé par les fuites. Toutefois, sa performance de détection n'est supérieure à ceile du CB que si le champ de bruit est hautement directionnel.

iii

TABLE OF CONTENTS

1. INTRODUCTION

1.1 STATEMENT OF THE PROBLEM

In underwater acoustics, as in other disciplines, a receiving array has definite advantages over the omnidirectional receiver for use in any data acquisition system. With the present capabilities of digital signal processors, data received at a many-sensor array can now be processed for on-line presentation of the features of the acoustic field.

Figure 1 displays a block diagram of a typical underwater acoustic data acquisition system, such as might be used in a passive sonar. Its principal components include a receiving array, a Fourier analyzer for determination of spectral features of the sound and an array beamformer for determination of its directional features. The digitized acoustic signals from the array hydrophones would be passed to a Fourier analyzer, for example the Discrete Fourier Transform (DFT), to permit frequency-domain presentation. The DFT essentially provides a bank of narrow filters stepped uniformly over the analysis frequency band. The multi-channel output of the Fourier analyzer is passed to a frequency-domain beamformer. The beamformer outputs a number of beams, the shapes of which depend on the array geometry, the beamforming algorithm, and the frequency. Hence at this stage the field can be monitored as a function of both frequency and direction. Of course, it is possible to interchange the order of the Fourier analyzer and beamformer, such that the beamforming is performed in the time-domain. However, the beam outputs will be essentially equivalent, regardless of this order.

At this point, the beam data may be further processed, according to one of two general purposes for the data acquisition. One is to produce a high-resolution mapping of the far-field directionality of the acoustic field. This is often the aim in research systems, where it is desirable to establish a data base of noise field directionality. Such information could be used to optimize or predict the signal detection performance of a future sonar. This suggests the second purpose of the data acquisition, namely the detection of signals against the noise. In this case, further processing might include setting a threshold for detection and comparing the beam output to the threshold. Both the spectral characteristics and directional characteristics of the signal would be exploited in the detection process. Signal detection is the ultimate aim of any sonar system.

In the past, signal processing was usually accomplished via a mix of specialized analogue and digital hardware. This processing was usually quite simple, which meant that the interpretation of the presented data was relatively straightforward. However, with the emergence of high-speed programmable digital array processors, the versatility and speed of signal processing has changed dramatically. The problem has now become one of thoroughly understanding how to interpret the output of this more sophisticated processing.
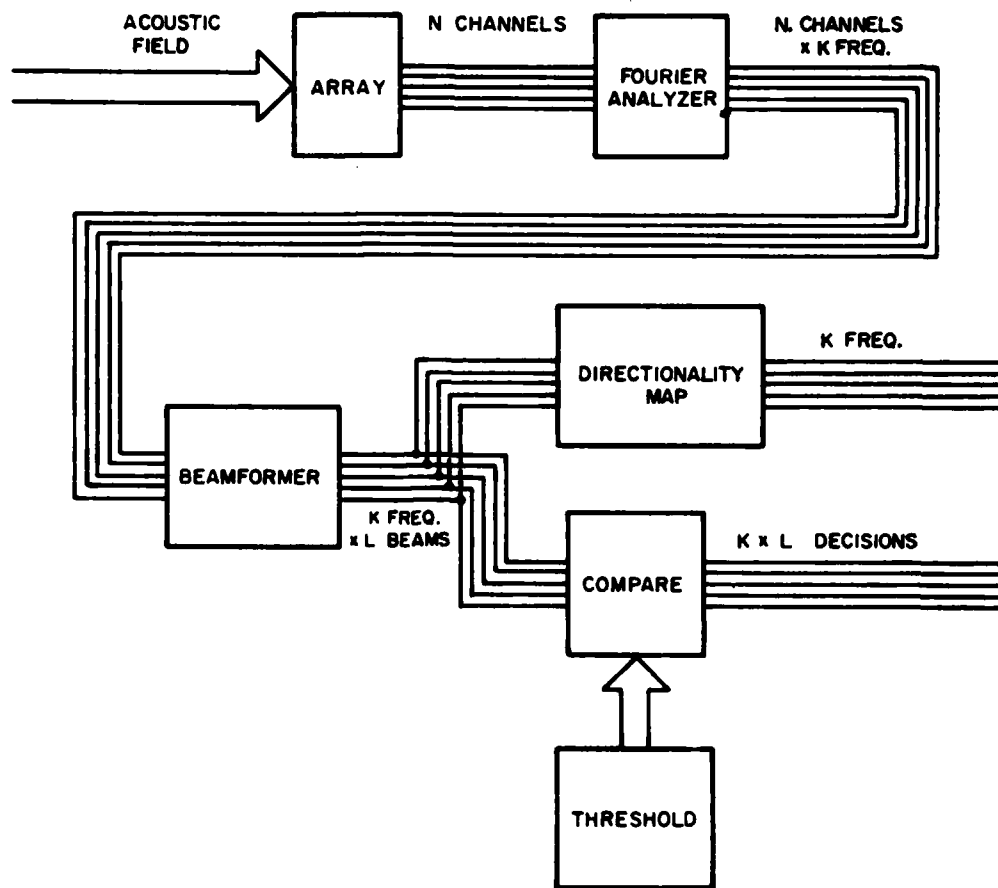
FIG. 1. Schematic of an underwater acoustics data acquisition system.

This report presents a mathematical and physical analysis of one component of the signal processing, namely the array beamformer. We will assume that the data presented to the beamformer has undergone Fourier analysis, such as indicated in Figure 1. We shall discuss how the choice of beamformer influences our interpretation of the processed data. The problem of interpretation is approached from the standpoints of both field directionality mapping and passive signal detection. We shall show that the choice of beamformer should be influenced by the purpose of the sonar. For example, in field directionality mapping, the aim is to obtain a high-resolution estimate of the true directionality, where the time-frame in which the estimate is obtained is of minor concern. The average direction-ality estimate is a convolution of the true directionality with the array directional response, or beampattern. Hence, the main factor to be con-sidered is the shape of the beampattern which the beamformer provides. On the other hand, in signal detection, a decision must be made within a finite time as to the presence or absence of a signal in a beam. Since the acoustic processes received at the array are stochastic, this time-frame can be so short that significant statistical variations in the esti-mates of the field are possible. Therefore, in addition to the array beam-pattern, we must also consider how the beamformer affects the confidence with which we can say that what looks to be a signal is not instead a statistical fluctuation in the noise. This then requires the determination of the beamformer statistics or, equivalently, its probability density function. As a final comment, we note that signal detection is similar to field directionality mapping under a time constraint.

1.2 FILLED VS. SPARSE LINE ARRAYS

Ultimately, the performance of a beamformer is limited by the geometry of the receiving array, because of the finite array aperture and/or number of sensors. Therefore, a study of array beamformers is usually specific to an array type.

An array geometry commonly used in sonar is a line of uniformly spaced omnidirectional hydrophones. This we refer to as a filled line array. The line array structure is comparatively easy to deploy, either as a vertical line suspended from a float, or as a horizontal line towed aft of a ship. From a signal processing standpoint, the array can pro-vide a large aperture, although its one-dimensional geometry only permits resolvability of the tilt angle from the array axis. The uniform sensor spacing is desirable for producing well behaved, symmetric beampatterns. As well, the uniform structure is suited to the vector operations avail-able within digital array processors.

However, if the number of hydrophones is fixed, the filled array geometry does not yield the maximum number of measurements of the spatial properties of the field that are possible. Hence, the maximum resolvabil-ity of the field is not achieved for the number of sensors. This results because of the redundancy inherent in the filled array due to the repeti-tion of sensor-pair spacings. Therefore, consideration is often given to

line arrays having less spatial redundancy than the filled line array. The question that arises is: how do these two types of line arrays differ in performance?

A sparse line array is produced by removing certain of the sensors from the filled array. When the eliminated sensors were only contributing to the spatially redundant measurements, then the sparse array will retain the directionality mapping capability of the filled line. In essence, the beampattern of the filled line array can be realized with fewer sensors. This economy, without a loss in the mapping capability makes the sparse array appear particularly attractive.

In general, a penalty is paid for the decrease in spatial redundancy associated with the sparse line array. This is a requirement to increase the time averaging, i.e. time redundancy, if we are to have the same confidence in the estimate of the field as compared to that of the filled array. Hence, while the sparse array may be well suited for directionality mapping, it may suffer in the signal detection application.

This report examines the properties of various beamformers suitable for beamforming both filled and sparse line arrays. The performance will be gauged in terms of both the ability to map the directionality and the ability to detect directional signals.

The standard for comparison will be the Conventional Frequency-Domain Beamformer (CB). It incorporates shading and linear phase shifting of the Fourier analyzed hydrophone signals. The shading controls the beampattern; the aim is to provide a narrow beamwidth but with low side-lobe levels. A second method to be examined measures the directionality by first estimating a function readily measurable with both filled and sparse arrays, namely, the spatial covariance function. It is well known that there exists a Fourier duality between this function and the directionality. The technique is analogous to the Cooley-Tukey method of time-series spectrum estimation via the Fourier transform of the auto-covariance function. (cf.1) For reasons we state later, this method will be referred to as the Principal Solution Beamformer (PSB). Finally, we shall discuss the data-adaptive methods that can be applied to filled and sparse array data processing. The term data-adaptive implies that the beamformer output is modified via feedback from the field measurements. Chosen for closer study is the Minimum Variance Beamformer (MVB). It uses the acquired data to estimate the array shading that will yield the beampattern having minimum sidelobe leakage.

1.3   SUMMARY OF THE SECTIONS

In Section 2, we shall discuss the restrictions which we impose on the sparse array geometry. The fewest number of sensors which can comprise a sparse array shall be restricted to a minimum-redundancy configuration, i.e. one which has the minimum repetition of sensor-pair spacings present in the filled array.

4

In Section 3, we develop the mathematics necessary to describe the directionality mapping problem in the case of both filled and sparse line arrays. We shall show in Section 3.1 the relationship between the directionality and one array measurement parameter, the cross-spectrum. The spatial covariance function is introduced as describing the dependence of the cross-spectrum on the sensor-pair spacing. For an infinitely long line of uniformly spaced sensors, the Discrete Fourier Transform (DFT) of the spatial covariance function yields the directionality. Since the line array is a finite extent of this line, the directionality can be estimated by measuring the spatial covariance function over the available aperture. In Sections 3.2 - 3.4, we shall examine the mathematics of three line array beamformers, i.e. the Conventional Beamformer (CB), the Principal Solution Beamformer (PSB), and the Minimum Variance Beamformer (MVB). We shall demonstrate that each maps the directionality via the DFT of a finite, windowed segment of the spatial covariance function. Hence, a comparison of these beamformers reduces to a comparison of the properties of the appropriate windows. We remark that the array beampattern is simply the DFT of this window.

The CB window is the autocovariance of the shading function which is chosen to weight each sensor. For the sparse array, we define this function as having zeroes at the positions of the sensors removed from the filled array. These zeroes introduce a degradation in the shape of the beampattern, thereby degrading the mapping capability. On the other hand, the PSB allows us to choose an arbitrary window. Hence, the mapping capabilities of the filled and sparse arrays can be made equal, simply by using the same window. The MVB window is directly dependent on the spatial properties of the field. It is chosen so as to minimize the leakage that occurs for each beam direction. Therefore, the MVB provides a field resolution that is superior to either the MVB or PSB. However, the window (and beampattern) is different for each beam; this significantly complicates the interpretation of the map.

The developments of Section 3 are made under the assumption of field homogeneity. Homogeneity implies that the cross-spectrum is invariant under coordinate translation of the sensor-pair measuring the cross-spectrum; it is this feature which allows the spatial redundancy of the filled array to be reduced without a loss in the ability of the array to map the directionality. However, when coherent multipath propagation conditions exist, as is often the case, the field can be highly inhomogeneous. In Section 4, we will examine the effects that inhomogeneity has on the beamformer mapping. The major effect for both the CB and the PSB is the introduction of a bias in the estimate of the bearings of correlated plane wave arrivals. In addition, the presence of inhomogeneity can lead to negative values in the PSB map. The ability of the MVB to resolve correlated arrivals is more seriously degraded since the MVB attempts to simultaneously null the signals.

In directionality mapping, the time-frame in which the map is obtained is of secondary concern. In fact, in the discussions of Sections 3 and 4, the time is assumed to be infinite, so only first-order

5

beamformer statistics are important. In practice, the time-frame must be finite, if for no other reason than to ensure stationarity of the field over the measurement period. Hence, the mapping obtained within this finite time will vary from the average mapping in a manner dependent on the higher-order beamformer statistics. This variation is commonly defined in terms of a confidence interval about the average. The estimate will lie within this interval 'with a given probability. In Section 5, we shall examine the confidence intervals appropriate for the various beamformers. It will be shown that while the PSB can allow the same directionality mapping for both the filled and sparse array, the confidence interval for the sparse arrry PSB estimate can be significantly wider than that for the filled array. Given the same array, the MVB has a wider confidence interval than the CB; this trade-off of stability for resolution is typical of the data-adaptive methods.

A natural extension of the discussion of confidence intervals is the problem of using the beamformer output for detection of directional signals. This is the topic of Section 6. We will point out that the signal detection performance of any beamformer depends on two parameters, namely the array gain and the detection threshold. The array gain is related to the directionality mapping capability of the array; the detection threshold is related to the width of the confidence interval. Ideally, we want a large array gain and a small detection threshold. The sparse array PSB generally has superior mapping capability compared to, say, the sparse array CB. How-ever, its confidence interval is such that it loses this advantage in the signal detection application. The MVB displays a similar trade-off. We shall examine conditions under which the MVB will have a detection perform-ance superior to that of the CB. In general, the more directional is the field, the clearer is the case for the MVB.

In summary, the following statements can be made based on the work presented in this report:

(1) if the performance criterion is the ability to map the field direc-tionality, the PSB has definite advantages over the CB for the sparse array beamforming (see Section 3);

(2) if performance is assessed in terms of the ability to detect direc-tional signals, the PSB should likely not be used in preference to the CB for sparse array beamforming (see Section 6);

(3) if there is evidence of field inhomogeneity and no significant source-receiver range rate exists, the MVB should not be used (see Section 4);

(4) the line array geometry which we recommend for use with the PSB is the minimum-redundant configuration (see Section 2); the geometry recom-mended for the MVB is the filled line (see Section 6);

(5) if the field is highly directional, the MVB will usually have a detection performance superior to that of the CB; if the field is approaching isotropic, the reverse is generally the case (see Section 6).

6

2. SPARSE ARRAY GEOMETRY

We shall consider a filled line array, having N equi-spaced hydrophones of intersensor separation, δ. A sparse line array results when one or more of the sensors are removed from the filled array structure. The array may be designed to maintain the total aperture of the filled array. It may also result by accident due to failure of one or more of the sensors in a filled array.

Considerations related to array performance criteria will place constraints on the sparse array geometry. For example, let us assume for the moment that the array performance is measured by the ability to map the field directionality. As will be discussed in Section 3, the spatial information on the field is embodied in the various cross-spectral estimates, $\hat{\Gamma}_{rs}(f)$, measured between all possible pairings of sensors r and s in the array. However, for a homogeneous acoustic field, the mean cross-spectra obtainable with the line array are unique only for different separations of the sensor pairs. For the N-sensor filled line array, values of sensor separation occur at integer multiples of the intersensor spacing, δ, i... :

$$d_{rs} = n\delta . \qquad 0 < n < N-1.$$

Because of the uniform structure of the array, each sensor separation, $n\delta$, occurs N-n times. Since for the homogeneous field the mean cross-spectra obtained for identical separations are the same, a spatial redundancy exists which will not improve the directionality mapping capability. On the other hand, this repetition of separations will reduce the time averaging necessary to be able to assign a specific confidence interval to the field estimate.

Since spatial redundancy does not directly affect the ability of the array to map the directionality, we may remove certain of the sensors from the filled array without penalty. The term, zero-redundancy, is applied to the sparse array for which each spacing, $n\delta$, occurs exactly once - except for n=0. Only a limited group of filled line arrays can be made zero-redundant; in general, only a minimum redundancy is attainable.[2] For N large, the number of sensors, L, in the minimum-redundancy configuration is bounded,[3] i.e.:

$$2.434 < L^2/N < 3.348 .$$

The line arrays for which numerical examples will be evaluated in this report are a filled array having N=10 sensors, and one of its two possible minimum-redundancy configurations, for which L=5. The minimum-redundancy configuration is shown schematically in Figure 2.

A real advantage of an array configuration based on a constant intersensor separation lies in the relative simplicity of its data processing algorithms, when compared to those required for a random sensor configuration. However, the maximum number of different separations available

FILLED $\overset{\displaystyle |\ \delta\ |}{\bullet\quad \bullet\quad \bullet\quad \bullet\quad \bullet\quad \bullet\quad \bullet\quad \bullet\quad \bullet\quad \bullet}$

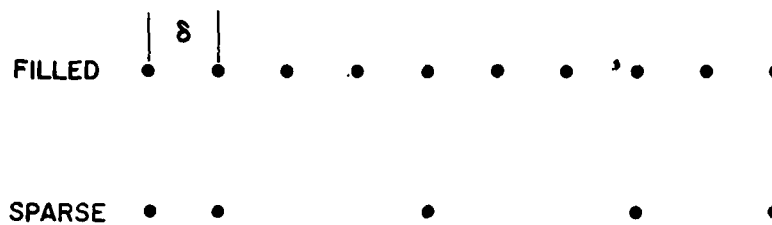SPARSE • •   •   •   •

FIG. 2.   Sparse array configuration.   Minimum-redundant configuration for 10
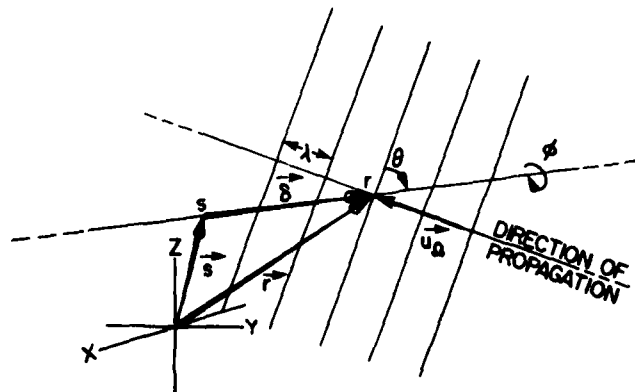sensor filled array of intersensor separation, δ.

FIG. 3.   Geometry. $\vec{u}_\Omega$ has been chosen to lie in the yz plane.

8

with an L-element-line array does not necessarily occur when the array is a minimum-redundancy configuration of a filled line array. If the constraint of uniform intersensor separation is removed, an infinite number of line array random configurations is possible, for which each sensor-pair separation is unique. The maximum number, K, of unique separations is then:

$$K = 1 + 1/2 \ L(L-1) \ .$$

3. MEAN ESTIMATION OF THE FIELD DIRECTIONALITY

In this section we will develop the relationship between the field directionality and one array measurement parameter, the cross-spectrum. Then we will examine the directionality mapping capabilities of various beamformers based on the cross-spectral estimates obtained with both filled and sparse line arrays.

3.1 CROSS-SPECTRUM/DIRECTIONALITY RELATIONSHIPS

Consider a line of infinite extent in an unbounded ocean medium. We locate on the line two points, r and s, whose positions are specified by vectors $\vec{r}$ and $\vec{s}$, respectively. The geometry is shown in Figure 3. The acoustic signal, $s_r(t)$, received by a hydrophone positioned at point r will be the integral over all angles of the signal arriving in solid angle, $d\Omega$, and from direction, Ω, specified by unit vector, $\vec{u}_\Omega$. Therefore, $s_r(t)$ becomes:

$$s_r(t) = \int\limits_{4\pi} p_\Omega(t - \vec{u}_\Omega \cdot \vec{r}/c) \ d\Omega \qquad , \qquad (1)$$

where it is assumed that the signal, $p_\Omega(t')d\Omega$, at the origin is a plane wave propagating at speed c, and in direction specified by the unit vector, $\vec{u}_\Omega$. Likewise, the signal, $s_s(t)$, at point s can be defined.

Assuming stationarity of the field, we define the cross-spectrum, $\Gamma_{rs}(f)$, for signals at r and s, and at frequency f, as:

$$\Gamma_{rs}(f) = \int\limits_{-\infty}^{\infty} \gamma_{rs}(\tau) \ e^{-j2\pi f\tau} \ d\tau \ , \qquad (2)$$

where $\gamma_{rs}(\tau)$ is the cross-covariance between $s_r(t)$ and $s_s(t-\tau)$:

$$\gamma_{rs}(\tau) = \ < s_r(t) \ s_s(t-\tau) > \ , \qquad (3)$$

$$= \gamma_{sr}(-\tau)$$

9

and <·> indicates expectation.

On insertion of Eq. (1) in Eq. (2) we obtain:

$$\Gamma_{rs}(f) = \int_{-\infty}^{\infty} \int_{4\pi} \int_{4\pi} <p_{\Omega}(t - \vec{u}_{\Omega} \cdot \vec{r}/c) p_{\Omega'}(t - \tau - \vec{u}_{\Omega'} \cdot \vec{s}/c)> e^{-j2\pi f\tau} d\Omega' d\Omega d\tau ,$$

(4a)

$$= \int_{4\pi} \int_{4\pi} P_{\Omega\Omega'}(f) e^{-j2\pi f(\vec{u}_{\Omega} \cdot \vec{r}/c - \vec{u}_{\Omega'} \cdot \vec{s}/c)} d\Omega' d\Omega ,$$

(4b)

where:
$$P_{\Omega\Omega'}(f) = \int_{-\infty}^{\infty} <p_{\Omega}(t) p_{\Omega'}(t-\tau)> e^{-j2\pi f\tau} d\tau.$$

(4c)

$P_{\Omega\Omega'}(f)$ is the complex covariance at f between the plane wave arrivals from Ω and Ω'. By imposing field homogeneity, we require that there be no correlated arrivals and hence that $P_{\Omega\Omega'}(f)$ be zero, except for $\Omega=\Omega'$, i.e.:

$$P_{\Omega\Omega'}(f) = P_{\Omega}(f) \qquad \Omega=\Omega' ,$$

$$= 0 \qquad \Omega \neq \Omega' ,$$

(5)

where $P_{\Omega}(f)$ is the power, or directionality, of the signal arriving from Ω. Then $\Gamma_{rs}(f)$ becomes:

$$\Gamma_{rs}(f) = \int_{4\pi} P_{\Omega}(f) e^{-j2\pi f\vec{u}_{\Omega} \cdot (\vec{r}-\vec{s})/c} d\Omega ,$$

(6a)

$$= \int_{4\pi} P_{\Omega}(f) e^{-j\vec{k} \cdot \vec{\delta}} d\Omega ,$$

(6b)

where $\vec{k}$ is the propagation vector, $\vec{k} = k\vec{u}_{\Omega}$, having wavenumber $k = 2\pi f/c$, and $\vec{\delta}$ is the separation vector, $\vec{\delta} = \vec{r}-\vec{s}$. Note that by assuming homogeneity, we reduce the dependence of the cross-spectrum on the absolute positions of r and s, to a dependence on the separation vector, $\vec{\delta}$, alone. Therefore, the cross-spectrum becomes independent of coordinate translation.

Since $\vec{u}_{\Omega}$ in Figure 3 has spherical coordinates $(1,\theta,\emptyset)$ relative to vector, $\vec{\delta}$, the cross-spectrum can be expressed as

$$\Gamma_{rs}(f) = \int_{-1}^{1} e^{jk\delta \sin\theta} d(\sin\theta) \int_{0}^{2\pi} P_{\Omega}(f) d\emptyset ,$$

(7a)

10

$$= \int_{-1}^{1} P_\Theta(f) e^{jk\delta \sin\Theta} d(\sin\Theta) \ . \tag{7b}$$

Angle Θ is the angle that the plane wavefront from $\vec{u}_\Omega$ makes with $\vec{\delta}$. $P_\Theta(f)$ is the integral of the power in all plane waves whose unit vectors have common angle, Θ.

Since $P_\Theta(f) = 0$ for $|\sin\Theta| > 1$, we choose to extend the limits of integration on Eq.(7b) to $\pm\pi/k\delta$, provided $k\delta \leq \pi$. We then recognize Eq. (7b) as an inverse Discrete Fourier Transform (DFT) in $k\delta$ and $\sin\Theta$. The corresponding forward DFT expresses the periodically-extended directionality, $P_\Theta'(f)$, in terms of the cross-spectra at separations equal to integer multiples of δ:

$$P_\Theta'(f) = \sum_{n=-\infty}^{\infty} \Gamma_n(f) e^{-jnk\delta\sin\Theta} \tag{(.)}$$

where

$$P_\Theta(f) = 0 \qquad\qquad |\sin\Theta| > \pi/k\delta \ ,$$

$$P_\Theta'(f) = P_\Theta(f) \qquad\qquad |\sin\Theta| \leq \pi/k\delta \ .$$

$\Gamma_n(f) = \Gamma_{j+n,j}(f)$, and is the cross-spectrum between sensors having separation, $n\delta$.

The duality between the cross-spectrum and directionality expressed by Eq. (8) is analogous to the duality between the autocovariance of a band-limited, stationary stochastic process and its power spectrum. Thus a plot of the cross-spectrum versus sensor separation may be referred to as the spatial covariance function. The constraint that $k\delta$ must be $\leq \pi$ is equivalent to requiring that $2\delta \leq \lambda$ (λ is the wavelength). This constraint is similar to the Nyquist sampling criterion that is applicable to sampled band-limited time-series (cf.1). It requires that the sampling frequency must be at least twice the upper bandedge frequency if the sampled time-series is to contain sufficient information to allow reconstruction of the original continuous process. When this condition is not met, frequencies above half the sampling frequency are folded, or aliased back into the band of interest. In the case of spatial sampling, the presence of spatial aliasing is manifested in the presence of grating lobes.

The similarity of the problem of directionality estimation and that of time-series spectrum estimation suggests that techniques developed for the latter problem can be extended to the former. Such extensions are the topic of Sections 3.2-3.4.

As implied by Eq. (8), one measurement parameter in directionality estimation is the cross-spectral estimator, $\hat{\Gamma}_{rs}(f,m)$, which we choose to define as:

$$\hat{\Gamma}_{rs}(f,m) = 1/m \sum_{p=1}^{m} X_{r,p}(f) X_{s,p}^{*}(f). \tag{9}$$

$(\cdot)^{*}$ is complex conjugation. $X_{j,k}(f)$ is the Fourier coefficient at f, obtained from a modified periodogram of length $T = L\Delta$ seconds, acting or the kth segment of the signal sampled at the jth point. Δ is the sampling interval, and m such segments are averaged. The operation described by Eq. 9 is indicated by the schematic of Figure 4. A potential problem with the method described by Eq. 9 can arise if the sensors are sufficiently separated, since the travel time, τ, between sensors may approach, or even exceed the DFT segment length, T. Should this occur, a significant bias can develop in the cross-spectral estimate. As an extreme example, consider a white broadband plane wave propagating along the line separating the sensors (endfire). If $\tau < T$, then the DFT samples at the sensors will be completely uncorrelated. Hence, the mean of the cross-spectral estimate will be zero, although the plane wave has complete spatial correlation. As the process becomes sufficiently "narrowband", or for the segment lengt!, T, sufficiently long, the estimator becomes essentially an unbiased estimator of the true cross-spectrum. In Appendix A, we attempt to quantify what constitutes sufficiently "narrowband".

By assuming the estimator, Eq. 9, is an unbiased estimator of the true cross-spectrum, we have:

$$< \hat{\Gamma}_{rs}(f,m) > = \lim_{m \to \infty} \hat{\Gamma}_{rs}(f,m) \sim \Gamma_{rs}(f). \tag{10}$$

3.2 CONVENTIONAL BEAMFORMER

The conventional beamformer (CB), as defined in this report, employs phasing to a plane and shading of the narrowband signals at each of the N sensors of the array. For an arbitrary array geometry, the conventional beampower estimate, $\hat{P}_{CB}(f,\Omega_0,m)$, at frequency, f, and for direction, Ω_0, can be expressed in the following matrix quadratic form:

$$\hat{P}_{CB}(f,\Omega_0,m) = \underline{A}^{\dagger}(f,\Omega_0)\underline{\hat{\Gamma}}(f,m)\,\underline{A}(f,\Omega_0) \tag{11}$$

$\underline{\hat{\Gamma}}(f,m)$ is the NxN matrix of m-sample cross-spectral estimates between all pairs of sensors in the array. $(\cdot)^{\dagger}$ indicates complex conjugate transpose. $\underline{A}(f,\Omega_0)$ is the array shading and steering vector, with components having the form:

$$A_n = a(n)e^{-j\vec{k}_0 \cdot \vec{d}_n}. \tag{12}$$

Vector $\vec{d}_n$ locates the nth sensor, and $\vec{k}_0$ is the propagation vector in direction, Ω_0. The $a(n)$ is the shading for the nth sensor, which may be complex.
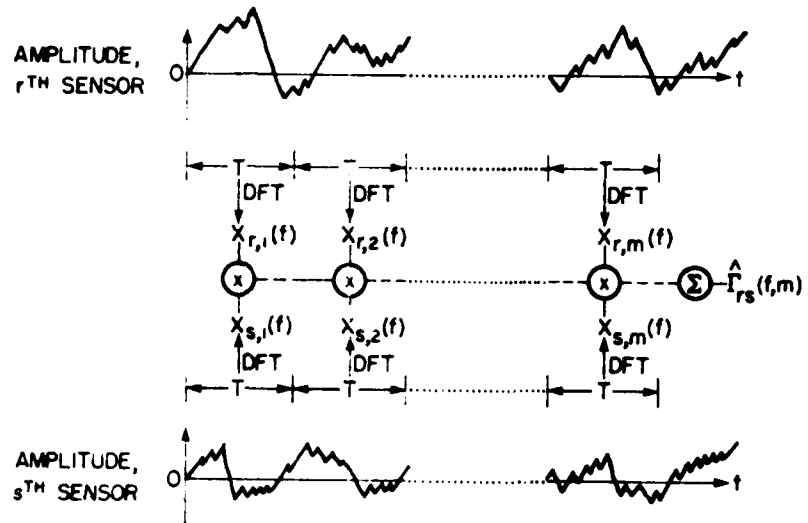
The expectation, $<\cdot>$, of the CB estimate is:

FIG. 4. Schematic of the operation of obtaining the cross-spectral estimate, $\hat{\Gamma}_{rs}(f,m)$.

$$\langle \hat{P}_{CB} (f,\Omega_0,m)\rangle = \underline{A}^{\dagger}(f,\Omega_0) \langle \hat{\underline{\Gamma}}(f,m)\rangle \underline{A}(f,\Omega_0) \qquad (13a)$$

$$= \sum_{p=1}^{N} \sum_{q=1}^{N} a^*(p)a(q) \langle \hat{\Gamma}_{pq}(f,m)\rangle e^{j\vec{k}_0 \cdot (\vec{d}_p - \vec{d}_q)} \qquad (13b)$$

where $\hat{\Gamma}_{jk}(f,m)$ is the j,k component of matrix $\hat{\underline{\Gamma}}(f,m)$.

If we assume field homogeneity, and that $\hat{\Gamma}_{jk}(f,m)$ is an unbiased estimator of the true cross-spectrum (see Appendix A), then $\langle \hat{\Gamma}_{jk}(f,m)\rangle$ is given by Eq. (6b). Upon substitution in Eq. (13), we obtain:

$$\langle \hat{P}_{CB}(f,\Omega_0)\rangle \sim \int_{4\pi} P_{\Omega}(f) [\sum_{p=1}^{N} \sum_{q=1}^{N} a^*(p)a(q)e^{-j(\vec{k}-\vec{k}_0) \cdot (\vec{d}_p - \vec{d}_q)}] d\Omega, \qquad (14a)$$

$$= \int_{4\pi} P_{\Omega}(f) \ B(\Omega,\Omega_0,f) d\Omega , \qquad (14b)$$

where the expectation of the beampower estimate is now independent of m. $B(\Omega,\Omega_0,f)$ is the array directional response, or beampattern, at frequency, f, and for direction, Ω_0.

3.2.1 Filled Line Array

Simplification of Eqs. (13) and (14) results when the array is a line of uniformly spaced sensors, having intersensor separation, δ. We shall position the origin of the coordinate system at one end of the array, and number the sensors increasing from one at the origin. The shading and steering vector, $\underline{A}(f,\Omega_0)$, now has components of the form:

$$A_n(f,\Theta_0) = a_F(n)e^{jk\delta(n-1)\sin\Theta_0} ,$$

where $a_F(n)$ is the shading for the nth sensor of the filled array. Θ_0 is the steering direction from array broadside, and is positive if the phase at the origin lags that at the other sensors. The CB estimate given by Eq. (11) reduces to:

$$\hat{P}_{CB}(f,\Theta_0,m) = \sum_{p=1}^{N} \sum_{q=1}^{N} a_F^*(p)a_F(q) \hat{\Gamma}_{pq}(f,m)e^{-jk\delta(p-q)\sin\Theta_0}, \qquad (15a)$$

$$= \sum_{n=-(N-1)}^{N-1} e^{-jnk\delta\sin\Theta_0} \Phi_F(f,m,n) , \qquad (15b)$$

14

where: $\quad \Phi_F(f,m,n) = \sum_{i=1}^{N-n} \hat{\Gamma}_{i+n,i}(f,m) \, a_F(i) a_F^*(i+n), \quad n \geq 0$ (15c)

$$= \Phi_F^*(f,m,-n) \quad , \qquad\qquad n < 0 \; .$$

$\Phi_F(f,m,n)$ is the weighted summation over the nth diagonal of the m-sample matrix of cross-spectral estimates (the main diagonal corresponds to n=0).

Again invoking field homogeneity and the narrowband assumption, we obtain the expectation of the CB estimate for the filled array as:

$$\langle \hat{P}_{CB}(f,\Theta_0) \rangle = \sum_{n=-(N-1)}^{N-1} w_F(n) \, \Gamma_n(f) \, e^{-jnk\delta\sin\Theta_0} \; , \qquad (16)$$

where: $\quad w_F(n) = \sum_{i=1}^{N-n} a_F(i) a_F^*(i+n), \qquad n \geq 0,$

$$= w_F^*(-n) \; , \qquad\qquad n < 0.$$

$\Gamma_n(f) \sim \langle \hat{\Gamma}_{i+n,i}(f,m) \rangle$ and is the cross-spectrum for the nth multiple of spacing, δ. Hence, the expectation of the beamformer estimate becomes independent of m. The window function, $w_F(n)$, is the autocovariance of the filled array shading function.

Eq. (16) is the Discrete Fourier Transform (DFT) of a finite, windowed segment of the spatial covariance function, with $k\delta$ and $\sin\Theta_0$ as transform variables. Note the similarity to Eq. (8), which states that the periodically-extended directionality, $P_\Theta'(f)$, is the DFT of the spatial covariance function. Hence, Eq. (15) can be expressed as a convolution in the $\sin\Theta_0$ domain:

$$\langle \hat{P}_{CB}(f,\Theta_0) \rangle = \int_{-\pi/k\delta}^{\pi/k\delta} P_\Theta'(f) \, B_F(\sin\Theta - \sin\Theta_0, f) \, d(\sin\Theta_0), \qquad (17)$$

where $P_\Theta'(f)$ is the periodically-extended directionality defined in Eq. (8), and the beampattern, B_F, is the DFT of the spatial covariance window function, $w_F(n)$. Note that the beampattern functional shape in the $\sin\Theta_0$ domain is independent of steering direction. Provided the spatial covariance function is adequately sampled ($\pi/k\delta \geq 1$), the integration limits can be confined to ± 1. If the spatial covariance function is undersampled ($\pi/k\delta < 1$), spatial aliasing of the directionality estimate will result.

With a redefinition of terms, it is apparent that the process of directionality mapping via the filled array CB is similar to the well-studied conventional methods of time series spectrum estimation.

3.2.2 Sparse Line Array

When sensors are removed from the filled array, the CB estimate for the resultant sparse array may be expressed in one of two ways:

1:
$$\hat{P}_{CB}(f,\Theta_0,m) = \underline{A}_S^\dagger(f,\Theta_0) \, \underline{\hat{\Gamma}}_S(f,m) \, \underline{A}_S(f,\Theta_0) \ , \tag{18}$$

where $\underline{\hat{\Gamma}}_S(f,m)$ is the LxL matrix of m-average cross-spectral estimates for the L-sensor sparse array ($L \leq N$). $\underline{A}_S(f,\Theta_0)$ is the L-component vector for sparse array steering and shading. The alternative expression is:

2:
$$\hat{P}_{CB}(f,\Theta_0,m) = \underline{A}_S^\dagger{}'(f,\Theta_0) \, \underline{\hat{\Gamma}}_F(f,m) \, \underline{A}_S{}'(f,\Theta_0) \ , \tag{19}$$

where $\underline{\hat{\Gamma}}_F(f,m)$ is the NxN matrix of cross-spectral estimates for the N-sensor filled array. Vector $\underline{A}_S{}'(f,\Theta_0)$ has N components, corresponding to the N sensor positions in the filled array, but with zero values occurring at the vector components corresponding to those sensors absent in the sparse array. That the sparse array does not permit the measure of all cross-spectra obtainable with the filled array is of no matter, since all such terms are given zero weight by the shading function.

The advantage of the second expression for the CB estimate is its similarity to that for the filled array. On performing the matrix operation defined by Eq. (19), we obtain:

$$\hat{P}_{CB}(f,\Theta_0,m) = \sum_{n=-(N-1)}^{N-1} e^{-jnk\delta\sin\Theta_0} \phi_S(f,m,n), \tag{20a}$$

where:
$$\phi_S(f,m,n) = \sum_{i=1}^{N-n} \hat{\Gamma}_{i+n,i}(f,m) a_S{}'(i) a_S{}^*{}'(i+n), \quad n \geq 0 \tag{20b}$$

$$= \phi_S^*(f,m,-n), \quad n < 0 \ .$$

The $a_S{}'(j)$ is the sparse array shading at the location of the jth sensor of the filled array, and is identically zero if the sensor is absent in the sparse array. On taking expectations, we have:

$$\langle \hat{P}_{CB}(f,\Theta_0) \rangle = \sum_{n=-(N-1)}^{N-1} w_S{}'(n) \, \Gamma_n(f) e^{-jnk\delta\sin\Theta_0}, \tag{21}$$

where:
$$\Gamma_n(f) \sim \langle \hat{\Gamma}_{i+n,i}(f,m) \rangle \ .$$

The window, $w_S{}'(n)$, is the autocovariance function of the N-component shading function given by the $a_S{}'(j)$'s.

Eq. (21) is identical to the expression for the mean of the
filled array CB estimate, Eq. (16), except for the form of the window
function. Expressed as a convolution in the $\sin\Theta_0$ domain, the mean CB
estimate is:

$$<\hat{P}_{CB}(f,\Theta_0)> = \int_{-\pi/k\delta}^{\pi/k\delta} P_\Theta'(f) B_S'(\sin\Theta - \sin\Theta_0, f) \, d(\sin\Theta), \qquad (22)$$

where the sparse array beampattern, B_S', is the DFT of the window, w_S'.

When sensors are removed from the filled array, we may attempt
to control the sparse array beampattern by adjustment of the shading
applied to the remaining sensors. For N large, and for several sensors
removed, the computations necessary to define the shading are non-trivial.[4]
An alternative method of shading that avoids this computation is to retain
the filled array shading at the remaining sensors. Then $a_S'(n) = a_F(n)$,
provided the nth sensor is present in the sparse array. In effect, this
describes the case where the CB acts on a filled array containing nulled
sensors when no compensating shading is applied. Later in the report, we
shall examine the performance of sparse array CB's that use this method of
shading.

3.3 PRINCIPAL SOLUTION BEAMFORMER

3.3.1 Filled Line Array

In the expression for the filled array CB estimate, Eq. (15b),
we observe that the estimate is dependent on the weighted sum of cross-
spectral estimates, where each summation occurs over a diagonal of the
cross-spectral matrix estimate. Suppose instead, we sum the cross-spectral
terms over the diagonal before applying a weighting function. This leads
to another estimate of the directionality, namely:

$$\hat{P}(f,\Theta_0,m) = \sum_{n=-(N-1)}^{N-1} u_F(n) e^{-jnk\delta\sin\Theta_0} \Theta_F(f,m,n), \qquad (23a)$$

$$\text{where:} \quad \Theta_F(f,m,n) = \sum_{i=1}^{N-n} \hat{\Gamma}_{i+n,i}(f,m) \qquad n \geq 0, \qquad (23b)$$

$$= \Theta_F^*(f,m,-n), \qquad n < 0.$$

$\Theta_F(f,m,n)$ is the summation over the nth diagonal of the m-sample matrix of
cross-spectral estimates (the main diagonal corresponds to n=0). The $u_F(n)$
is an arbitrary spatial covariance window of non-zero value only for
$|n|<N$.

17

Again assuming field homogeneity and narrowband signals, the expectation of the above estimate is:

$$\langle \hat{P}(f,\Theta_0) \rangle = \sum_{n=-(N-1)}^{N-1} u_{F'}(n) \; \Gamma_n(f) e^{-jnk\delta\sin\Theta_0}, \qquad (24)$$

where: $\Gamma_n(f) \sim \langle \hat{\Gamma}_{i+n,i}(f,m) \rangle$,

and $u_{F'}(n) = (N-|n|) u_F(n)$.

Some observations can be made from a comparison of the above estimator and the CB estimator:

(1)   the estimate, Eq. (23), is analogous to the Blackman-Tukey method of time-series spectrum estimation, (cf.1) where the summation, Θ_F, is the equivalent of the autocovariance estimator at the nth time lag and $u_F(n)$ corresponds to the autocovariance lag window;

(2)   the means of the directionality estimators, Eqs. (16) and (24), will be identical, provided the window functions are set equal, and the assumptions made in defining the means are correct. While no restriction need be placed on the form of $u_{F'}(n)$, the CB window, $w_F(n)$, is restricted in form, since it must be an autocovariance function. Therefore, mean directionality estimates can be obtained via Eq. (24), which are not realizable via conventional beamforming;

(3)   an obvious example of (2) above, is the case where $u_{F'}(n)$ equals a constant for $|n| < N$, since there is no shading function which has a rectangular autocovariance function. The resultant beampattern for the rectangular window is a Sinc function. Although having poor sidelobe behaviour, it has the narrowest beamwidth possible of an important class of windows, namely those having $u_{F'}(n) \geq 0$ and $u_{F'}(j) \leq u_{F'}(k)$, $j > k$. The mean directionality estimate obtained via Eq. (24) and using the rectangular window, is referred to as the principal solution[5] for the field. Therefore, we shall refer to the directionality estimator, Eq. (23), as the Principal Solution Beamformer (PSB), $P_{PSB}(f,\Theta_0,m)$, although we will not restrict the definition to only the rectangular window;

(4)   while the means of the CB and PSB estimators will be identical for identical windows, higher order moments will generally not be the same;

(5)   because of the quadratic form of the CB operator, and since the cross-spectral estimate is positive semi-definite, the CB estimate is unconditionally non-negative. This is, of course, provided the cross-spectral matrix estimate is not ill-conditioned by measurement errors, such as quantization. However, the PSB estimate may be negative, with a probability that is dependent on the field direction-

ality and spatial covariance window. For windows which yield beam-patterns possessing negative sidelobes, it is also possible that the mean of the PSB estimate will be negative;

(6) if the beampattern of the PSB window is non-negative for all bearings, then we may define its square root, although not uniquely. The inverse DFT of any of these square root functions defines an array shading which has the spatial covariance window as its autocovariance. Hence, if the PSB beampattern is non-negative there must exist an array shading from which the beampattern may be obtained. Therefore, a CB can be defined, which will yield the same mean estimate as the PSB.

3.3.2 Sparse Line Array

For the filled array PSB estimate as given by Eq.(23), the spatial covariance at the nth multiple of spacing, δ, is estimated via a summation over the N-n cross-spectral estimates available for that separation. If the field is homogeneous, the cross-spectrum need be measured at only one of these N-n spacings in order to retain the spatial information. The measurements at the remaining spacings provide spatially redundant information, which will not improve the ability to map the field. Therefore it is possible to form a sparse line array which can provide the mapping capability of the filled array. The restriction on sparse array geometry is that each of the N-1 multiples of spacing, δ, that are present in the filled array, must occur at least once. As was discussed in Section 2, the geometry which meets this restraint with the fewest number of sensors in the sparse array is referred to as the minimum-redundancy configuration[2].

The sparse array PSB estimate is:

$$\hat{P}_{PSB}(f,\Theta_0,m) = \sum_{n=-(N-1)}^{N-1} u_S(n)e^{-jnk\delta\sin\Theta_0}\,\Theta_S(f,m,n) \ , \qquad (25a)$$

where: $\quad \Theta_S(f,m,n) = \sum_{i=1}^{N-n} \hat{\Gamma}_{i+n,i}(f,m)\varepsilon_i\varepsilon_{i+n}, \quad n \geq 0 \ , \qquad (25b)$

$$= \Theta_S^* \ (f,m,-n) \ , \qquad\qquad n < 0 \ .$$

The $\varepsilon_j = 0$ or 1, depending on whether the jth sensor of the filled array is absent or present in the sparse array. The $u_S(n)$ is an arbitrary spatial covariance window for the sparse array.

The mean of the PSB estimate is:

$$\langle\hat{P}_{PSB}(f,\Theta_0)\rangle = \sum_{n=-(N-1)}^{N-1} u_{S'}(n)\Gamma_n(f)e^{-jnk\delta\sin\Theta_0} \ , \qquad (26)$$

19

where: $\Gamma_n(f) \sim \langle\hat{\Gamma}_{i+n,i}(f,m)\rangle$,

and $\qquad u_{S'}(n) = u_S(n) \sum\limits_{i=1}^{N-n} \epsilon_i \epsilon_{i+n} = u_S(n)K(n)$.

$K(n)$ is the number of repetitions of spacing n within the sparse array, and must be at least one. When the window, $u_{S'}(n)$, is the triangular window, $N-|n|$, the sparse array PSB estimate given above is equivalent to the field estimator discussed in Reference 6 using its "default combination coefficients".

By equating $u_{S'}(n)$ to the filled array CB window, $w_F(n)$, we realize the important property of the PSB estimator; namely, the sparse array can provide the same directionality map as the filled array. Therefore, sensor failure within a filled array need not mean a loss of array performance, if performance is assessed on this mapping capability. However, it is important to realize that higher order statistics of the sparse array PSB estimate will not be the same as those of the filled array CB estimate. For continuity, we state now two general observations which we make later in the report:

(1) the variance of the sparse array PSB estimate will likely be larger than that of the filled array estimate. Therefore, the sparse array performance will be inferior to that of the filled array, should the array be the receiver for a signal detection device. Such performance is the topic of Section 6;

(2) also in Section 6, we show that while the mean of the sparse array PSB estimate will be non-negative for a proper choice of spatial covariance window, there may be a non-zero probability of obtaining negative directionality estimates.

3.4 MINIMUM VARIANCE BEAMFORMER

A beamformer can be termed data adaptive if its operation is altered so as to satisfy some optimality criterion that is applied to the measurements of the actual acoustic field. Examples of data adaptive beamformers are the Minimum Variance Beamformer[7] (MVB), the Maximum Entropy Method[8], and Discrete Field Decomposition[9]. All are characterized as non-linear operators, which can produce a superior resolution of the field when compared to a linear operator, such as the CB. Generally, there is a trade-off, namely an increased resolution for a decreased stability, or increased variance, of the estimate. Therefore, the data adaptive beamformers may be well suited to achieving performance criteria based on field mapping ability, but less well suited when the performance criterion imposes a time constraint.

The MVB can be chosen for study as typical of the class of data adaptive beamformers. The MVB optimality criterion is the maximization of

the array output signal to noise ratio, or array gain (AG), subject to the
constraint that a plane wave signal arriving in the beam direction must
pass undistorted through the beamformer. Maximization of array gain is
achieved via minimization of the array noise gain, hence the term Minimum
Variance.

The MVB estimator attempts to achieve the optimality criterion
as follows. Suppose we wish to measure the power arriving from a particu-
lar bearing as accurately as possible. This will be achieved by obtaining
the power in the look direction exactly, while at the same time adjusting
the array beampattern so as to minimize leakage of power from all other
bearings. The MVB uses the maximum likelihood criterion applied to the
cross-spectral matrix estimate, in order to estimate the array shading
necessary to obtain this optimum beampattern.

The MVB estimate can be expressed in a form similar to that of
the CB estimate, i.e.:

$$\hat{P}_{MVB}(f,\Omega_0,m) = \underline{\hat{\alpha}}^\dagger(f,\Omega_0,m)\underline{\hat{\Gamma}}(f,m)\underline{\hat{\alpha}}(f,\Omega_0,m) \quad , \tag{27}$$

where $\underline{\hat{\Gamma}}(f,m)$ is the NxN matrix of m-sample cross-spectral estimates.
Vector $\underline{\hat{\alpha}}(f,\Omega_0,m)$ is an estimate of the (complex) weight vector which
achieves the MVB optimization criterion. If the true cross-spectral matrix
$\underline{Q}(f)$, for the noise field alone, were known, the optimum vector would be
given by:[7]

$$\underline{\alpha}(f,\Omega_0) = \frac{\underline{Q}^{-1}(f) \ \underline{S}(f,\Omega_0)}{\underline{S}^\dagger(f,\Omega_0) \ \underline{Q}^{-1}(f) \ \underline{S}(f,\Omega_0)} \quad . \tag{28}$$

$(\cdot)^{-1}$ indicates matrix inversion. $\underline{S}(f,\Omega_0)$ is the array steering vector,
whose nth component has the form:

$$S_n(f,\Omega_0) = e^{-j\vec{k}_0 \cdot \vec{d}_n} \quad , \tag{29}$$

where $\vec{k}_0$ is the propagation vector for direction, Ω_0, and $\vec{d}_n$ locates the
nth sensor. Implicit in the solution for the optimum weight vector is an
assumption of field homogeneity. The effects of the invalidity of this
assumption are examined in Section 4.

In general, $\underline{Q}(f)$ is not known a priori. There are a variety of
methods[10] of estimating the optimum weight vector, $\underline{\alpha}(f,\Omega_0)$. The most
direct method, referred to as the Sample Matrix Inversion (SMI) method[11],
is to substitute the cross-spectral matrix estimate $\underline{\hat{\Gamma}}(f,m)$ for $\underline{Q}(f)$ in
Equation (28), i.e.:

$$\underline{\hat{\alpha}}(f,\Omega_0,m) = \frac{\underline{\hat{\Gamma}}^{-1}(f,m) \ \underline{S}(f,\Omega_0)}{\underline{S}^\dagger(f,\Omega_0)\underline{\hat{\Gamma}}^{-1}(f,m) \ \underline{S}(f,\Omega_0)} \quad . \tag{30}$$

21

On substitution of Equation (30) into Equation (27), we obtain the MVB estimate:

$$\hat{P}_{MVB}(f,\Omega_O,m) = \frac{\underline{S}^\dagger(f,\Omega_O)\underline{\hat{\Gamma}}^{-1\dagger}(f,m)\underline{\hat{\Gamma}}(f,m)\underline{\hat{\Gamma}}^{-1}(f,m)\underline{S}(f,\Omega_O)}{[\underline{S}(f,\Omega_O)\underline{\hat{\Gamma}}^{-1}(f,m)\underline{S}(f,\Omega_O)]^2} \quad , \qquad (31a)$$

$$= [\underline{S}^\dagger(f,\Omega_O)\underline{\hat{\Gamma}}^{-1}(f,m)\underline{S}(f,\Omega_O)]^{-1} \quad . \qquad (31b)$$

Assuming that the sensor signals are narrowband Gaussian, it can be shown[12] that the expectation of Equation (31) is proportional to the mean of the estimate that would be obtained if the optimum weights were known a priori, i.e.:

$$<\hat{P}_{MVB}(f,\Omega_O,m)> = [(m-N+1)/m]\underline{\alpha}(f,\Omega_O)<\underline{\hat{\Gamma}}(f,m)>\underline{\alpha}(f,\Omega_O) \quad (m \geq N) \qquad (32)$$

$$\sim [(m-N+1)/m]\underline{\alpha}(f,\Omega_O)\underline{\Gamma}(f)\underline{\alpha}(f,\Omega_O) \quad .$$

The factor in [·] introduces a bias in the estimate. It goes to zero as the number of samples, m, increases. Thus, the Sample Matrix Inversion method provides a consistent estimate of the mean of the MVB estimate that would be obtained if the optimum weights were known a priori.

3.4.1 Filled Line Array

For an N-sensor uniform line array of intersensor separation, δ, the MVB estimate expressed by Equation (31b) can be written:[7]

$$P_{MVB}(f,\Theta_O,m) = [\sum_{n=-(N-1)}^{N-1} e^{-jnk\delta\sin\Theta_O}\psi_F(f,m,n)]^{-1} \quad , \qquad (33a)$$

where

$$\psi(f,m,n) = \sum_{i=1}^{N-n}\hat{g}_{i+n,i}(f,m) \quad , \quad n \geq 0 \quad , \qquad (33b)$$

$$= \psi_F^*(f,m,-n), \quad n < 0 \quad ,$$

and $\hat{g}_{jk}(f,m)$ is the j,k component of the NxN matrix inverse of the cross-spectral matrix estimate, $\underline{\hat{\Gamma}}(f,m)$.

It is instructive to express the filled array MVB estimate in a form similar to that of the CB and PSB estimators, namely:

$$\hat{P}_{MVB}(f,\Theta_O,m) = \sum_{n=-(N-1)}^{N-1}\hat{v}_F(n,m)e^{-jnk\delta\sin\Theta_O}\Theta_F(f,m,n) \qquad (34)$$

where $\Theta_F(f,m,n)$ is defined in Equation 23b. The window $\hat{v}_F(n,m)$, is an estimate of the optimum spatial covariance window for the MVB, and is given by:

$$\hat{v}_F(n,m) = \sum_{i=1}^{N-n} \hat{\alpha}_F(i,m)\hat{\alpha}_F^*(i+n,m)e^{jnk\delta\sin\Theta_0} \quad n \geq 0 \qquad (35a)$$

$$= \frac{\sum_{i=1}^{N-n}\sum_{p=1}^{N}\sum_{q=1}^{N} \hat{g}_{ip}(f,m)\hat{g}_{i+n,q}^*(f,m)e^{-j(p-q)k\delta\sin\Theta_0}}{[\sum_{p=1}^{N}\sum_{q=1}^{N} \hat{g}_{pq}(f,m)e^{-j(p-q)k\delta\sin\Theta_0}]^2} \qquad (35b)$$

$$= \hat{v}_F(-n,m) \qquad n < 0 \quad .$$

For the homogeneous field, the expectation of the MVB estimate, Equation (34), becomes:

$$<\hat{P}_{MVB}(f,\Theta_0,m)> = [(m-N+1)/m](\sum_{n=-(N-1)}^{N-1} v_F(n)\Gamma_n(f)e^{-jnk\delta\sin\Theta_0}) \quad ,(36)$$

where $\qquad \Gamma_n(f) \sim <\hat{\Gamma}_{i+n,i}(f,m)> \quad .$

The spatial covariance window, $v_F(n)$, is obtained by replacing the terms, $\hat{g}_{jk}(f,m)$, of the matrix inverse estimate in Equation (35b) by those of the true matrix inverse.

We observe that the window is a function of the properties of the field, through $\hat{g}_{jk}(f,m)$, and also of the look direction. Consequently, the functional form, or shape of the beampattern will be dependent on these parameters. This is unlike the beampatterns of the CB and PSB estimators discussed in Sections 3.2 and 3.3. This property makes it difficult to qualitatively assess the influence that power from other directions is having on the MVB beampower.

It can be shown[7] that the resolution of the field obtainable with the MVB is superior to that obtainable with the beamformers discussed earlier. Graphical examples of the MVB resolution capabilities are given in Section 4.

Examples of MVB performance for some special but important types of fields can be readily examined. If the field consists of noise that is uncorrelated from sensor to sensor, the cross-spectral matrix is diagonal. Then the MVB window, $v_F(n)$, reduces to the triangular window, $v_F(n) = N - |n|$. This window is the same as would result for the CB using a uniform array shading. Therefore the CB using a uniform array shading must be optimum in terms of array gain, if the noise field consists of spatially uncorrelated noise. As a second example, we assume the field consists of N or fewer independent plane waves, each having a different bearing. The MVB beampattern will place nulls at the bearings of all plane waves not in the beam, i.e.: the MVB will exactly resolve N or fewer plane waves. Essentially, this is a consequence of the fact that the cross-spectral matrix can have up to N unique eigenvalues.

3.4.2 Sparse Line Array

The sparse line array MVB estimate is:

$$\hat{P}_{MVB}(f,\Theta_O,m) = \hat{\underline{\alpha}}_S^{\dagger}(f,\Theta_O,m)\hat{\underline{\Gamma}}_S(f,m)\hat{\underline{\alpha}}_S(f,\Theta_O,m) \ , \tag{37}$$

where $\hat{\underline{\Gamma}}_S(f,m)$ is the LxL matrix of m-sample cross-spectral estimates for the L-sensor sparse array $(L \leq N)$. $\hat{\underline{\alpha}}_S(f,\Theta_O,m)$ is the estimate of the L-component optimum weight vector. It is obtained via an equation of the form of Equation (30), with the appropriate sparse array matrices substituted.

For the sparse array CB estimate, the formulation of the beam-former was made similar to that of the filled array CB by redefining the spatial covariance window. Likewise, the sparse array MVB estimate can be made similar to that for the filled array by an adjustment of the MVB spatial covariance window for the sparse array. The adjusted window is obtained by adding a large number to the autopower terms of the filled array cross-spectral matrix that correspond to those sensors that are missing in the sparse array. The number added must be large relative to the autopower. When the inverse of such a matrix is performed, the effect is to zero the rows and columns that intersect at the autopower locations of the missing sensors. This results in the nth window term being made zero if the nth sensor is missing in the sparse array, thereby removing the sensor from the beamformer calculations.

The above technique is useful in treating the situation of sensor failure within the filled line array, since minimal adjustment is required in the MVB algorithm. However, if an N-sensor line array is to be designed to use the MVB, the question becomes: what is the best sensor geometry for the line array? While the minimum-redundant sparse array geometry has advantages if the PSB is to be used, this is not necessarily the case if the MVB is chosen. It is expected that the best geometry will depend on the field directionality, frequency and number of sensors; therefore, there will be no geometry that will be best for all cases. We suggest that a useful geometry will be the N-sensor filled line array, having intersensor separation, δ, such that $k\delta = \pi$. In Section 6, we will compare the performance of the MVB acting on both an N-sensor filled line array and N-sensor minimum-redundant array.

24

4. THE EFFECTS OF FIELD INHOMOGENEITY

The analytic expressions for the field maps assume that the acoustic field is homogeneous. Homogeneity was seen in Section 3.1 to require that the complex covariance, $P_{\Omega\Omega'}(f)$, between plane waves from Ω and Ω' must assume the form:

$$P_{\Omega\Omega}(f) = P_{\Omega}(f)\delta(\Omega-\Omega').$$

However, the assumption of homogeneity may be invalid for two reasons. First, the receiver may be in the near field so that the assumption of plane wave propagation breaks down. This is generally less of a problem than the second reason, where because of the depth dependent sound velocity profile in the ocean, and since the medium is bounded by the ocean surface and bottom, a variety of paths may exist for transport of acoustic energy from a source to receiver. At the lower frequencies, volume and surface scattering of the propagating sound may be insufficient to destroy the coherence among the various paths. The result of such propagation is that an interference pattern will be displayed by the autopowers measured at the various sensors of the array. We note that this coherence is effectively destroyed when there exists a significant range rate between the source and receiver, such that sufficient cycles of the interference pattern are averaged within the integration time. Suitable range rates are common when the array is towed, as might be a horizontal line array. Therefore, the problem of inhomogeneity may be more severe for stationary structures, such as a vertical line array.

We shall assume the field contains M narrowband plane waves, which arrive at the array from M unique bearings, plus a homogeneous directionality component. The covariance, $P_{pq}(f)$, between the pth and q^{th} waves, can be written as:

$$P_{pq}(f) = |P_{pq}(f)| \, e^{j\phi_{pq}} = (P_p(f)P_q(f))^{\frac{1}{2}}|\rho_{pq}|e^{j\phi_{pq}} \quad . \tag{38}$$

$P_j(f)$ is the power in the jth wave, ϕ_{jk} is the relative phase at the origin between the jth and k^{th} waves, and $|\rho_{jk}|$ is the magnitude correlation coefficient. Then from a discrete version of Equation (4b), the cross-spectrum, $\Gamma_{rs}(f)$, between points r and s, becomes:

$$\Gamma_{rs}(f) = \sum_{p=1}^{M} \sum_{q=1}^{M} P_{pq}(f) \, e^{-j(\vec{k}_p\cdot\vec{d}_r - \vec{k}_q\cdot\vec{d}_s)} + \Gamma_{rs}(f)\Big|_h \,, \tag{39a}$$

$$= \sum_{p=1}^{M} \sum_{q=1}^{M} [P_p(f)P_q(f)]^{\frac{1}{2}}|\rho_{pq}|e^{j(\phi_{pq}-\vec{k}_p\cdot\vec{d}_r+\vec{k}_q\cdot\vec{d}_s)} + \Gamma_{rs}(f)\Big|_h \,. \tag{39b}$$

25

$\Gamma_{rs}(f)\big|_h$ is the contribution to the cross-spectrum due to the homogeneous component of the field. If the array is a filled line array of intersensor separation, δ, the cross-spectrum between points having separation $(r-s)\delta$ reduces to:

$$\Gamma_{rs}(f) = \sum_{p=1}^{M} \sum_{q=1}^{M} [P_p(f)P_q(f)]^{\frac{1}{2}} |\rho_{pq}| e^{j(\emptyset_{pq} - k\delta(r \cdot \sin\Theta_p - s \cdot \sin\Theta_q))}$$
$$+ \Gamma_{r-s}(f)\big|_h, \quad (40)$$

where Θ_j is the bearing of the jth plane wave to the array broadside. While the component of the cross-spectrum due to the homogeneous part of the field depends only on the sensor separation, $(r-s)\delta$, the component due to the inhomogeneous part is dependent on the absolute sensor locations. Therefore, the spatial redundancy present when the line array is immersed in the homogeneous field does not exist when the field is inhomogeneous. This suggests that the sparse array may no longer be able to return the same map of the field as the filled array.

An example of the effects of field inhomogeneity on the mean of the CB estimate is shown in Figure 5. The array used in the calculations is a filled line array of N=10 sensors, having an intersensor separation, δ, such that $k\delta = 3\pi/4$. The array has a uniform sensor shading. The acoustic field has been modelled to consist of two plane waves of equal power, from directions of 10° and 45° re array broadside, and a three-dimensional isotropic noise at a total power 20dB below the maximum signal power. The mean of the CB estimate is obtained by substituting the cross-spectra defined by Equation (40), for the cross-spectral estimates of Equation (15b). Figure 5 plots the mean beampower, or directionality map, as a function of the look direction from array broadside. The beampowers have been normalized by the quantity, 1/C, where:

$$C = \left[\sum_{n=-(N-1)}^{N-1} w_F(n) \right] P_S = \left[\sum_{j=1}^{N} a_F(j) \right]^2 P_S . \quad (41)$$

P_S is the power in each of the signals. The normalization adjusts the beampattern so that its value in the look direction is $1/P_S$.

Directionality maps have been plotted in Figure 5 for the cases where the two signals are completely uncorrelated, $|\rho_{12}| = 0$, and where the signals are completely correlated, $|\rho_{12}| = 1$. The phase is arbitrarily set at $\emptyset_{12} = 50°$. We observe that the introduction of inhomogenity through correlation of the signals does not strongly affect the map of the signal powers when the array is steered to precisely their true directions. However, apparent shifts of the beampower maxima have occurred. Without a knowledge of the presence of the inhomogeneity we would be led to erroneous estimates of the signal powers and bearings. Similar behaviour occurs for the sparse array CB.
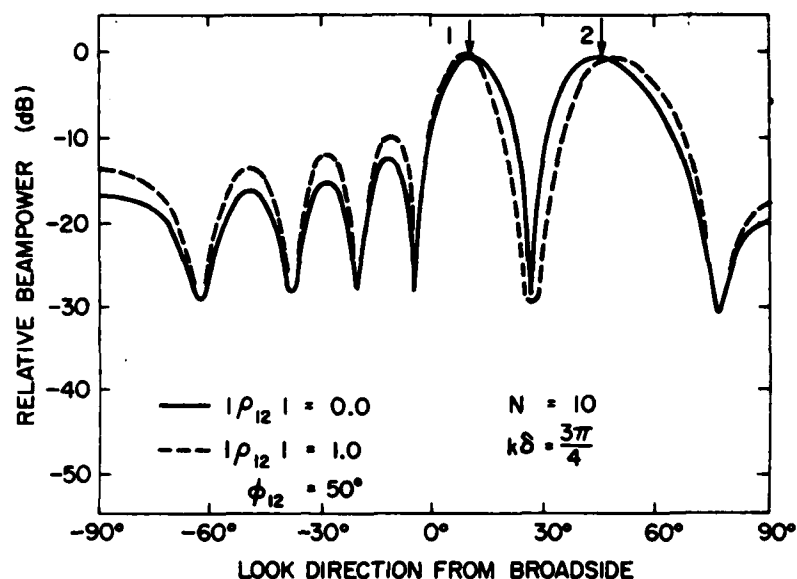
FIG. 5. Expectation of the filled array CB estimate for N = 10 sensors, and
for kδ = 3π/4. Field consists of plane waves at 10° and 45° from
broadside and of equal power, and isotropic noise of total power
20 dB below the signal power. Solid line - magnitude correlation,
$|\rho_{12}| = 0$; dashed line - $|\rho_{12}| = 1$, phase - $\phi_{12} = 50°$.

27

The important property of the sparse array PSB is its ability to return the same map of the field directionality as the filled array, provided the field is homogeneous. When inhomogeneity exists, such is no longer the case. An example of this effect is given in Figure 6. The sparse array has 5 sensors, and is one of the two possible minimum-redundancy configurations of a 10-sensor filled array of intersensor separation, δ. Its geometry is shown in Figure 2. Separation, δ, has been chosen so that $k\delta = 3\pi/4$. The field is modelled to consist of three narrowband plane waves at bearings of -60°, 10° and 40° re array broadside, and of relative powers of -3, 0 and 0 dB, respectively. Included in the field is a homogeneous component consisting of three-dimensional isotropic noise at a total power 13 dB below the maximum signal power. Note that Equation (21) is inappropriate for the mean of the PSB estimate when the field is inhomogeneous. Hence, the mean must be calculated by substituting the cross-spectra obtained via Equation (40) for the cross-spectral estimates of Equation (20). A triangular spatial covariance window, $u_{S'}(n) = N - |n|$, has been used. Therefore, when the field is homogeneous the mean of the PSB estimate will be the same as that obtained from the CB for the 10-sensor uniformly-shaded filled line array. Beampowers have been normalized by $1/C$, where:

$$C = [\sum_{n=-(N-1)}^{N-1} u_{S'}(n)] \, P_S , \qquad (42)$$

and P_S is the maximum signal power.

Figure 6 shows the PSB directionality map for three values of correlation between signals 1 and 2 ($|\rho_{12}|=0,0.5$ and 1). The phase is arbitrarily set at $\phi_{12} = 50°$. The principal effect caused by the presence of inhomogeneity is an unreliability in the map at bearings that are removed from the predominant directional sources. Negative beampowers are predominant over these bearings. The extent of the pattern breakdown is comparable for $|\rho_{12}| = 0.5$ and for $|\rho_{12}| = 1$. The effect of inhomogeneity on the estimates of the plane wave bearings and powers is similar to the effects we observed for the CB estimate; namely shifts in the signal peaks occur which will lead to erroneous bearing estimates.

Figure 6 demonstrates a rather severe test on the performance of the PSB in an inhomogeneous field, since the array considered in the calculations was minimum-redundant. Obviously, the mean of the PSB estimate will approach that for the filled array as the repetition of spacings increases. For spacings where repetition does exist, the cross-spectral summation, $\theta_S(n)$, of Equation (25) can be made to more closely resemble that for the filled array. This may be achieved by interpolating estimates for missing cross-spectra between those cross-spectra that are present at the particular spacing.[13]
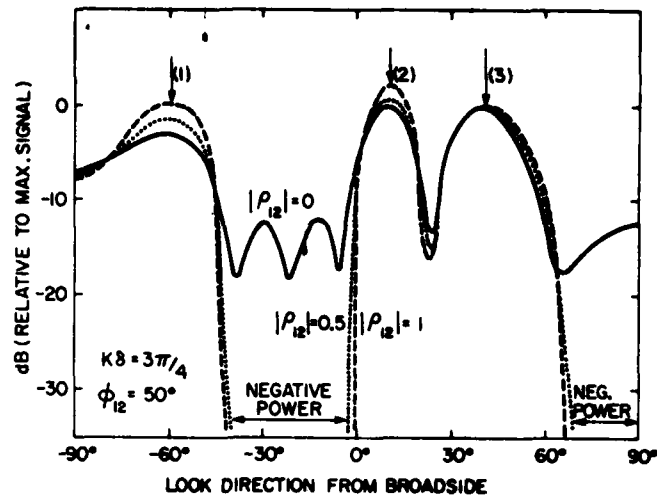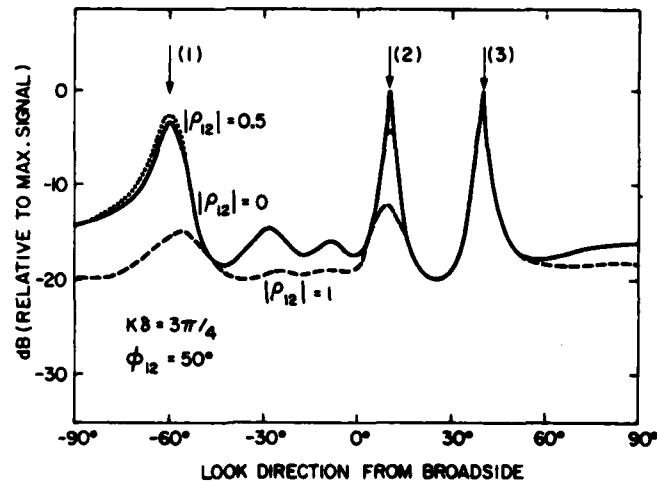
FIG. 6. Expectation of the sparse array PSB estimate for the sparse array
geometry indicated in Figure 2, and for $k\delta = 3\pi/4$. Field consists of
three plane waves whose directions from broadside and relative powers
are (-60°,3 dB), (10°,0 dB) and (45°,0 dB), plus isotropic noise of
total power 13 dB below the maximum signal power. Solid line -
magnitude correlation, $|\rho_{12}| = 0$; dotted line - $|\rho_{12}| = 0.5$, phase -
$\phi_{12} = 50°$; dashed line - $|\rho_{12}| = 1$, phase - $\phi_{12} = 50°$.

FIG. 7. Expectation of the sparse array MVB estimate for the sparse array
geometry indicated in Figure 2, and for $k\delta = 3\pi/4$. Field and signal
correlations same as in Figure 6.

29

Figure 7 presents plots of the MVB directionality map for the same field model and array geometry as was assumed for Figure 6. The beampowers have been normalized so that the maximum power equals 0 dB. When the field is homogeneous, the resolution obtained is obviously superior to that obtainable with either the PSB or the CB. However, as correlation is introduced between signals 1 and 2, the magnitudes of the correlated signals are observed to decrease. This mutual nulling of the estimates of correlated signals is an inherent difficulty with the MVB[14]. However, the estimate of the remainder of the field suffers little distortion.

5. CONFIDENCE INTERVALS

In Section 3, we formulated three methods (CB, PSB and MVB) of beamforming for both filled and sparse line arrays. Expressions for the field maps for the beamformer were derived on the assumption of field homogeneity. We demonstrated that the maps could all be described as the DFT of a finite, windowed segment of the spatial covariance function. One method, the PSB, allows the sparse array to return the same map as the filled array CB. Thus, when no time constraint is imposed, the sparse array field mapping capability is identical to that of the filled array.

In practice, of course, the time interval available for the beamformer to produce the field map is not infinite. When a time constraint is imposed, an uncertainty is introduced in the beamformer output. This uncertainty can be quantified in terms of a confidence interval about the expected value, that has an assigned probability of containing the estimate. In this section, we compare the confidence that can be assigned to the field estimates obtained via the various beamformers for both filled and sparse arrays. The parameter for comparison will be the variance of the estimates. This avoids the problems involved in calculating the probability density functions for the beamformer estimates, which would be necessary if the confidence intervals were to be calculated exactly. However, as the averaging time increases, the density functions will approach Normality, according to the Central Limit Theorem[15]. The Normal density function is characterized by its mean and variance; hence, the use of variance alone to describe the confidence has validity for sufficient averaging.

We shall assume that the acoustic signals received at the sensors of the array can be described as narrowband zero-mean complex Gaussian stationary stochastic processes, of equal variance at each sensor. The assumption of equal variance is equivalent to an assumption of field homogeneity.

For the above assumptions, the CB estimate, Equation (13), is Chi-Square distributed[12], with a number of degrees of freedom, $f_\nu = 2m$, where m is the number of independent DFT segments that have been used to obtain the various cross-spectral estimates. The variance of the estimate is given by:

$$\sigma_{CB}^2(f,\Omega_o,m) = \frac{<\hat{P}_{CB}(f,\Omega_o)>^2}{m} .$$ (43)

Thus, if the mean of the estimate is known, the variance is specified by Equation (43). Therefore, the variance is dependent on the array geometry, the field directionality and the frequency, to the same degree as is the mean of the estimate. We note that for the Chi-Square density function, all higher order moments can as well be expressed in terms of the mean.

In general, the statistics of the PSB estimate cannot be expressed in closed form. However, in Appendix B, we have derived the analytic expression for the variance, σ_{CB}^2, of the PSB estimate for both the filled and sparse line arrays. When the array is filled and a triangular spatial covariance window is chosen, the variance reduces to Equation (43), i.e. that for the CB using a uniform sensor shading. This is expected since a comparison of the expressions for the filled array CB and PSB estimates reveals they are identical for the above choice of windows. For any other spatial covariance window and/or sparse array geometry, this equivalence no longer exists. Then the proportionality between the mean and variance of the PSB estimate becomes dependent on the array geometry, the properties of the field, the window and the frequency.

In Section 3.3, we observed that by appropriately choosing the spatial covariance window, the sparse array PSB directionality map could be made identical to the filled array CB map. The condition on the PSB window was that it must be the autocovariance of the filled array sensor shading. However, while the maps may be the same, their variances may be quite different. This difference can be expressed by the ratio of the variances, which we define as:

$$\beta(f,\Theta_o) = 5 \log [\sigma_{PSB}^2(f,\Theta_o,m)/\sigma_{CB}^2(f,\Theta_o,m)],$$ (44)

$$= 5 \log [\sigma_{PSB}^2(f,\Theta_o,1)/\sigma_{CB}^2(f,\Theta_o,1)].$$

The variance ratio, β, is independent of the number of samples, m, provided m is the same for both beamformers. In effect, this ratio defines the approximate fractional change in integration time that would be necessary for the sparse array PSB beampower estimate to exhibit the same confidence as the filled array CB estimate. The parameter, β, is plotted in Figures 8 and 9 as a function of $k\delta$ and for various steering directions, Θ_o. δ is the intersensor separation in the filled array, and k is the wavenumber. Array broadside corresponds to $\Theta_o = 0°$. The arrays used in these calculations are the 10-sensor filled array and 5-sensor minimum-redundant array indicated in Figure 2.
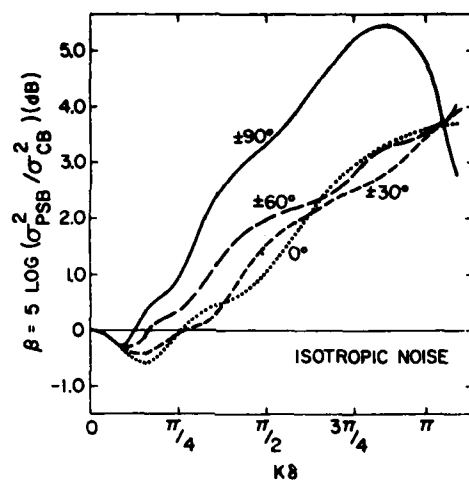
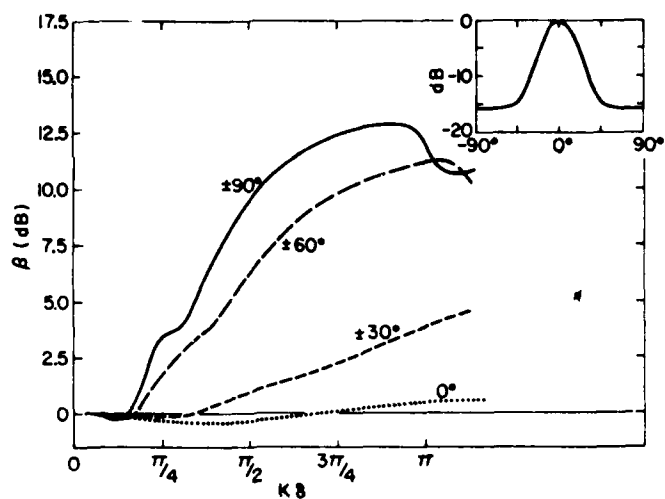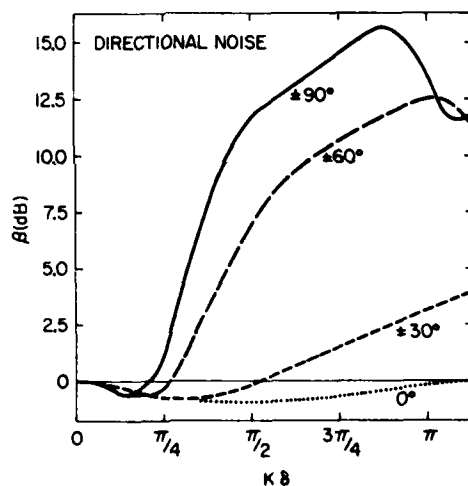8a. Uniform sensor shading;
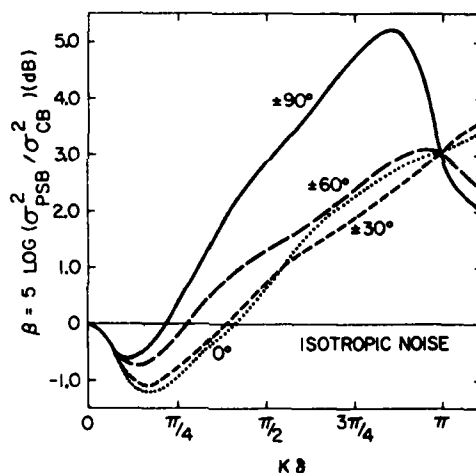
8b. Taylor shading, with the first sidelobe 30 dB down.

FIG. 8. Variance ratio, β, defined by Equation (44), as a function of $k\delta$, and for various steering directions. CB uses 10-sensor filled array; PSB uses the 5-sensor sparse array of Figure 2. Field consists of isotropic noise.

32

9a. Uniform sensor shading;

9b. Taylor shading, with the first sidelobe 30 dB down.

FIG. 9. Variance ratio, β, as a function of kδ, and for various steering
directions. CB uses the 10-sensor filled array; PSB uses the
5-sensor sparse array of Figure 2. Field consists of lobe
symmetrically distributed about broadside plus isotropic noise.
Relative directionality is indicated in the insert.

Different acoustic fields have been modelled in the two figures. Figure 8 presents the case where the field consists of three-dimensional isotropic noise[16]. Figure 9 corresponds to a field that is composed of an isotropic component plus a directional lobe that is symmetrically distributed about array broadside. The latter component is representative of the vertical directionality associated with noise due to distant shipping in the 50-200 Hz acoustic band[17]; the cross-spectra due to this component have been modelled according to Stockhausen[18] The relative field directionality is indicated in the insert in Figure 9a.

Two types of sensor shading have been used in the calculations for each of Figures 8 and 9. Figures 8a and 9a result when the filled array has a uniform sensor shading. Therefore the sparse array PSB uses a triangular spatial covariance window. Figures 8b and 9b result when the filled array uses a Taylor sensor shading[19], where the first sidelobe of the beampattern is 30 dB below the main lobe. The sparse array PSB window in this case will be the autocovariance of the Taylor shading function.

We observe that for $k\delta \lesssim \pi/2$, β may be negative, indicating that $\sigma^2_{PSB} < \sigma^2_{CB}$. For the types of field directionality modelled in Figures 8 and 9, the variance ratio goes to unity as $k\delta$ approaches zero, since the signals at each sensor become completely correlated. It can be shown that the variance ratio is a local maximum at $k\delta = 0$; therefore, the variance ratio will be less than unity for $k\delta$ near zero. From a physical standpoint, the implication is that we obtain at a specific $k\delta$, a more confident estimate of the field using the sparse array PSB than is possible with the filled array CB. Such behaviour will be likely under a wide variety of conditions, since *the CB in no way attempts to minimize the variance on its estimate.*

Generally, the values of $k\delta$ over which a specific array is to operate range from $\pi/2 \leq k\delta \leq \pi$. For a fixed number of sensors, a decrease in $k\delta$ causes a broadening of the beampattern, with a resulting decrease in resolution. For $k\delta > \pi$, the spatial covariance function is undersampled, and aliasing of the field estimate results. Within this somewhat limited range of $k\delta$ values, we observe in Figures 8 and 9 that the variance ratio can be very large. The ratio is greatest near array endfire, and also at bearings away from dominant directional components. For example, in Figure 9a the variance of the sparse array PSB estimate is seen to exceed that for the filled array CB by as much as 13 dB. This difference means that a 400-fold increase in the sparse array PSB integration time would be necessary for its estimate of the field to lie within the same confidence interval as the filled array CB estimate. Overall, the choice of window function appears to have only a secondary influence on the variance ratio, provided the window is well-behaved.

Besides the dependence of the variance ratio on the field directionality and window function, the ratio will also be affected by the sparse array geometry. The influence of geometry on the variance ratio is examined in Figure 10. We assume that the filled array uses a uniform
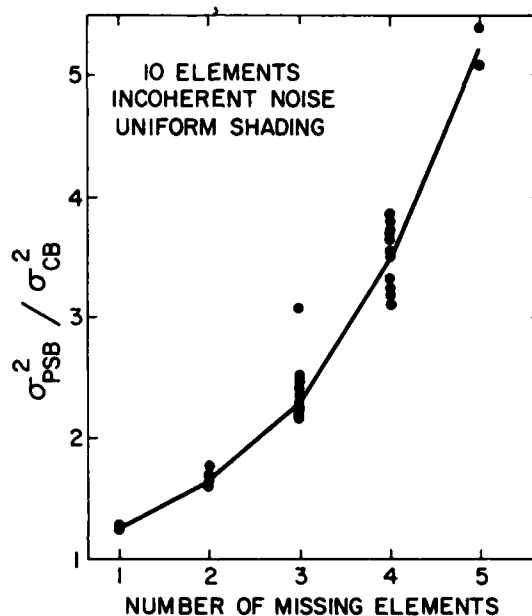
FIG. 10. Variance ratio as a function of sparse array configuration. CB uses 10-sensor filled array having a uniform sensor shading. Field consists of spatially uncorrelated noise. Points indicate variance ratio for each permutation of the sparse array configuration. Solid line is average of the ratios.

3 5

shading, and that the field consists of noise that is uncorrelated from sensor to sensor. Then the variance ratio becomes:

$$\sigma_{PSB}^2/\sigma_{CB}^2 = 1/L + 1/N[\sum_{n=1}^{N-1}(N-n)/\sum_{i=1}^{N-n}\varepsilon_i\varepsilon_{i+n}] \ , \tag{45}$$

where N and L are the number of sensors in the filled and sparse arrays, respectively, and ε_j=0 or 1, depending on the absence or presence of the jth filled array sensor in the sparse array. We see that for a field consisting solely of incoherent noise, the variance ratio is independent of Θ_o and $k\delta$. The points of Figure 10 represent the solution of Equation (45) for N=10 sensors and for each permutation of L sensors of the sparse array within the same total aperture as the filled array, and such that each of the N-1 spacings in the filled array occurs at least once. For N=10, L must be at least 5 in order that the restraint on spacing occurrence is met. The solid line of Figure 10 shows the average of the ratios over all permutations possible at each L. The influence of permutation on the variance ratio appears to be less significant than the influence of the factors examined in Figures 8 and 9.

As was the case for the CB estimate of the field the MVB estimate, Equation (31b), has been demonstrated to have Chi-Square statistics[12], but with a number of degrees of freedom, $f_v = 2(m-N+1)$. Therefore, the variance, σ_{MVB}^2, of the estimate is:

$$\sigma_{MVB}^2(f,\Theta_o,m) = \frac{<\hat{P}_{MVB}(f,\Theta_o)>^2}{m-N+1} \qquad (m \geq N) \tag{46}$$

The number of samples, m, must exceed or equal the number of sensors, N, since this is a necessary condition[7] for there to exist an inverse of the cross-spectral matrix estimate, $\underline{\Gamma}(f,m)$. The fewer degrees of freedom associated with the statistics of the MVB estimate means a larger confidence interval on the estimate, when compared to that of the CB estimate. Therefore, we have traded stability of the estimate for the improved resolution of the field when we choose the MVB over the CB. For m>>N, the relative loss of stability is negligible.

6. THE DETECTION OF NARROWBAND PLANE WAVE SIGNALS

So far we have compared the performance of array beamformers in terms of their ability to map the field directionality. Suppose now the beampower estimate is to be input to a detector which will test for the presence of a narrowband plane wave signal at the frequency, f, of the beampower estimate, and in the direction, Ω_0, of the beam. Such is the case in passive sonar. Typically, this will impose a time constraint on the estimation problem, which may significantly alter our perception of the beamformers' relative performance.

The detector will compare the beampower estimate to a threshold power, T_0, to test for one of two hypotheses: the beam contains a signal if the beampower $\geq T_0$; the beam does not contain a signal if the beampower $< T_0$. For the standard parametric decision model, T_0 is determined a priori based on knowledge of the probability density functions which describe the statistics at the beamformer output when either noise alone or signal plus noise is present at the beamformer input. The detection statistics, i.e. probability of false alarm, P_{fa}, and probability of detection, P_D, can be assigned to T_0, by integration of the appropriate density functions beyond the threshold.

6.1 BEAM NOISE STATISTICS

We shall assume that the acoustic noise present at each sensor is a stationary, homogeneous, zero-mean Gaussian stochastic process, that has a power spectrum that is broadband and flat relative to the bandwidth of each DFT bin. Then the DFT output, $X_{j,k}(f)$, in the bin at frequency, f, for the jth sensor and kth data segment will be zero-mean complex Gaussian, and uncorrelated from segment to segment. These assumptions lead us to the Chi-Square density function for the CB and MVB estimates of the noise component of the field[12], a result identical to the statistics of these estimators proposed in Section 5.

In general, the statistics of the PSB estimate of the noise field are not characterized by a convenient closed-form analytic expression. One relatively simple method of examining the PSB noise statistics, which does not require an analytic solution, makes use of Monte Carlo techniques (cf.20). The application of Monte Carlo techniques to the determination of density functions is outlined in Appendix C.

Shown in Figure 11 are some examples of the density function of the PSB estimate of the noise field for specific (f,Θ_0). The functions have been estimated using the Monte Carlo methods discussed in Appendix C for 10^4 trials. The functions correspond to one sample, i.e. m = 1, and have been smoothed by eye for ease of plotting. The sparse array has the 5-sensor minimum-redundancy configuration indicated in Figure 2. Each function has been normalized by its mean. This normalization has the advantage that the density function of the CB is represented by a single
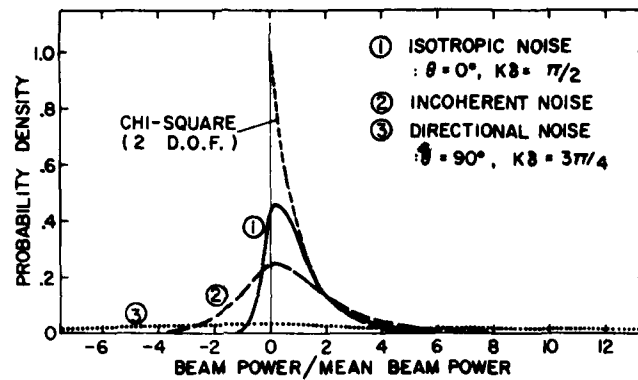
37

FIG. 11.   Probability density functions of the beampower estimates for the
          filled array CB and for the sparse array PSB. Sparse array is the
          5-sensor array of Figure 2. Number of samples, m = 1.
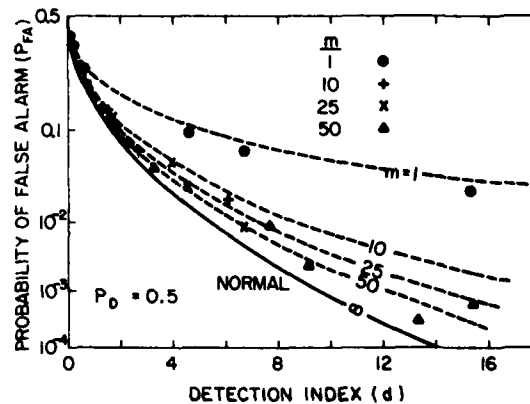

FIG. 12.   Probability of false alarm, P_{fa}, for a plane wave signal in the beam
          versus detection index, DI, and with the probability of detection,
          $P_D = 0.5$. Solid line - beamformer estimates of noise and of signal
          plus noise have Normal statistics; dashed lines - beamformer estimates
          have Chi-square statistics with 2m degrees of freedom; points - Monte
          Carlo calculations of the density functions of the PSB estimate for
          various sets of parameters.

unique curve, e^{-y}, (Chi-Square, 2 degrees of freedom), irrespective of Θ_0, $k\delta$, array geometry and field directionality. It is the dashed curve in Figure 11. This uniqueness does not exist for the PSB density function, as demonstrated by the remaining curves. Each gives the statistics of the PSB estimate that would be obtained for a particular Θ_0, $k\delta$ and field directionality; the parameters corresponding to each function are indicated in the figure. One function is given for each of the acoustic fields modelled in Figures 8-10. Note that since the PSB is not a positive semi-definite quadratic operator, as is the CB, there exists a non-zero probability of obtaining a negative power estimate.

Any attempt to exactly parameterize detection statistics from density functions such as curves 1-3 of Figure 11 will be impractical because of the number of parameters necessary to uniquely specify each function. However, since some averaging will likely be necessary in order to achieve realistic detection probabilities, the Central Limit Theorem will eventually ease the problem. When the function becomes approximateiy Normal, only its mean, variance (for one sample) and number of samples need be known for its characterization.

6.2 BEAM SIGNAL PLUS NOISE STATISTICS

The determination of the density function for the beampower estimate in the presence of signal plus noise requires a model of the statistics of the narrowband signal. The appropriate model is dependent on the acoustic propagation conditions that exist over the source-receiver separation.(cf.21) One of the three following models is often assumed:

(1) the signal has an unknown phase at each sample and has a deterministic amplitude. The density function for signal plus noise power at each sensor has a non-central Chi-Square distribution;(cf.22)

(2) the signal has an unknown phase and a Raleigh fluctuating amplitude that is highly correlated over the m DFT segments. This is referred to as a Swerling Type I fluctuating signal;(cf.23)

(3) the signal has an unknown phase and a Raleigh fluctuating amplitude that is uncorrelated among the m DFT segments. This is referred to as a Swerling Type II fluctuating signal.(cf.24) We note that thi⁊ model is equivalent to assuming the signal is a complex narrowband Gaussian signal that is centered on the DFT bin, and has a bandwidth matched to the bandwidth of the DFT bin. This results in the statistics of the beamformer estimate in the presence of signal plus noise being identical to those in the presence of noise alone, since the signal appears to be noise-like in all aspects but its directionality.

Regardless of the model that we assume for the signal, when sufficient averaging has occurred, the density functions will approach Normality. The detection statistics appropriate when the density functions

39

are Normal are completely described by two parameters. One is the detection index, DI, defined as[22]:

$$DI = (<\hat{P}_{S+N}> - <\hat{P}_N>)/\sigma^2(\hat{P}_N) \tag{47}$$

where $\hat{P}_{S+N}$ and $\hat{P}_N$ indicate the beamformer estimate of the signal plus noise and noise powers respectively. The second parameter is the ratio, r_v, of the variances of the beamformer estimates in the presence of signal plus noise and of noise alone[22], i.e.:

$$r_V = \sigma^2(\hat{P}_{S+N})/\sigma^2(\hat{P}_N). \tag{48}$$

Let us use the third of the models for the signal, and examine how quickly the density functions of the beamformer estimates approach Normality. Plotted in Figure 12 is the dependence of the false-alarm probability, P_{fa}, on the detection index, DI, when the probability of detection, P_D, is fixed at 0.5. Since the Normal distribution is symmetric, and since we choose P = 0.5, one unique curve will describe the dependence of P_{fa} on DI, provided the density functions for the beamformer estimates of noise and signal plus noise are Normal. This single curve is the solid line of Figure 12. The dashed lines present the dependence of P_{fa} on DI when both density functions are Chi-Square distributed. This would be the case for the CB and MVB estimates. Note that if both functions are Chi-Square, the variance ratio, r_V, becomes the ratio of the squares of the means of the estimates. The curves in Figure 12 are parameterized by the number of degrees of freedom $f_v = 2m$. The data points are obtained from density functions for the PSB estimate that have been calculated using Monte Carlo techniques. Each point is the result of calculations based on a specific set of parameters, such as field directionality, kδ and direction. Since the density functions depend on a variety of parameters, a unique curve is not to be expected for each m. However, it appears that the density functions of the PSB estimate approach Normality about as quickly as when the estimates are Chi-Square distributed.

6.3 BEAMFORMER PERFORMANCE

When the beamformer is to be used for narrowband plane wave signal detection, it is obviously desirable that the beamformer enhance the ratio of the signal and noise powers at its output, relative to the ratio at its input. This enhancement is referred to as array gain, AG, and is expressed in decibels as:

$$AG(f,\Omega_O) = 10 \log \left[\frac{<\hat{P}_S>/<\hat{P}_N> \text{ array output}}{<\hat{P}_S>/<\hat{P}_N> \text{ array input}}\right] \tag{49}$$

$<\hat{P}_S>$ and $<\hat{P}_N>$ are the expectations of the estimates of the powers of signal and noise, respectively.

We shall term the CB array gain obtained using the filled array as AG_F and using the sparse array as AG_S. Generally, AG_S will be less than AG_F, due to the possible degradation of the array beampattern when the number of sensors decreases. For example, the degraded beampattern may have a broader main lobe, which will accept more noise than the narrower main lobe of the filled array beampattern.

Suppose the sparse array is beamformed using the PSB instead of the CB. Then the same directionality map as the filled array CB will be obtained, provided the PSB window function is the autocovariance of the filled array sensor shading. The AG provided by the sparse array PSB must then equal that of the filled array CB; hence, the PSB would appear more desirable than the CB for beamforming with the sparse array.

However, AG does not entirely define the beamformer performance in the signal detection application, since it does not consider the effect of the time constraint. Typically, this effect is included in another parameter, the detection threshold, DT. This parameter must be considered in conjunction with the AG, in order to completely quantify the beamformer performance. DT can be defined as the decibel ratio of the beamformer estimate of the signal power in the DFT bin, to the beamformer estimate of noise in a 1 Hz band, which must be achieved in order to assign specific P_D and P_{fa}. As the averaging time increases, the statistics of the beamformer estimates approach Normality, and DT is given by[22]:

$$DT = 5 \ \log \frac{B \cdot DI}{T} = 5 \ \log \frac{B^2 \cdot DI}{m} . \tag{50}$$

T is the integration time and B is the bandwidth of the DFT bin. The detection index, DI, is defined in Equation (47).

If T and B are fixed, a comparison of the detection thresholds appropriate for the various beamformers reduces to a comparison of the detection index, DI, necessary for the beamformer outputs to exhibit identical detection statistics.

We shall assume a P_D = 0.5, since if the density function of the estimate of signal plus noise is Normal, this will avoid the necessity of specifying a model for the signal. Therefore, only the statistics of the beamformer estimate of the noise field require consideration.

It is evident from the equations which describe the CB estimate of the noise field that the statistics of the estimate will have a density function of the same functional form, regardless of whether the array is filled or sparse. Therefore, the detection index is identical for both arrays, and a comparison of AG alone is sufficient to define the relative performance of the CB for the two arrays.

While the sparse array PSB directionality map may be identical to that obtained with the filled array CB, the variances of the

41

estimates are not. This suggests that a difference in detection thresholds will exist which, for Normal statistics, is given by:

$$DT_{PSB} - DT_{CB} = 5 \log \left[\frac{DI_{PSB}}{DI_{CB}}\right] = 5 \log \left[\sigma^2_{PSB}/\sigma^2_{CB}\right] . \qquad (51)$$

Equation (51) may be recognized as the parameter, β, introduced in Section 5. We observe that an increase by amount, β, in the integration time used in obtaining the PSB estimate will offset this difference in thresholds.

Whether the PSB or CB is the better choice for beamforming with the sparse array can be determined by the following. We define a parameter, $\propto$, as the difference in the sparse array CB gain and the effective sparse array PSB gain:

$$\propto = AG_S - (AG_F - \beta) \qquad (52)$$

$$= \beta - AG_F + AG_S .$$

For a specific set of conditions, i.e. $k\delta$, array geometry and shading, and noise field directionality, if this parameter is negative, superior detection performance will be obtained by using the PSB, rather than the CB, for beamforming with the sparse array.

The parameter, $\propto$, has been plotted in Figures 13 and 14. The array we consider is the 5-sensor minimum-redundant array of Figure 2. The sparse array CB uses the shading function of the filled array but with the weights for missing sensors set to zero. This method was discussed in Section 3.3. The noise fields and window functions considered in the calculations for Figures 13 and 14 are identical to those considered in Figures 8 and 9, namely: isotropic or directional noise (see Figure 9a) and uniform or Taylor shading functions.

Such plots reveal that $\propto$ is sensitive to the choise of θ_0 and $k\delta$, even for relatively well-behaved noise fields. While $\propto$ will specify which beamformer is preferred for a specific set of conditions, it is obvious that even a minor change in these conditions can reverse the preference. Therefore, we conclude that there is no obvious detection advantage by beamforming the sparse array with the PSB instead of the CB.

Owing to this conclusion, the ultimate decision as to the worth of PSB implementation must lie in whether there is a relative ease in realizing its structure. A significant problem is the necessity of knowing a priori the PSB statistics, which may require estimation of moments other than the mean. For long integration times, this reduces to estimation of its mean and variance. Unfortunately, the problem of variance estimation is not trivial, with the penalty being decreased processor speed and increased storage. One may avoid the problem of variance estimation by assuming knowledge of the noise field directionality that will
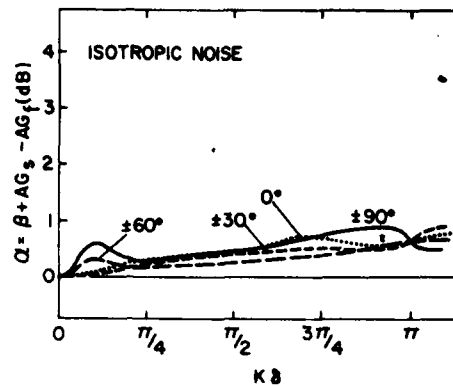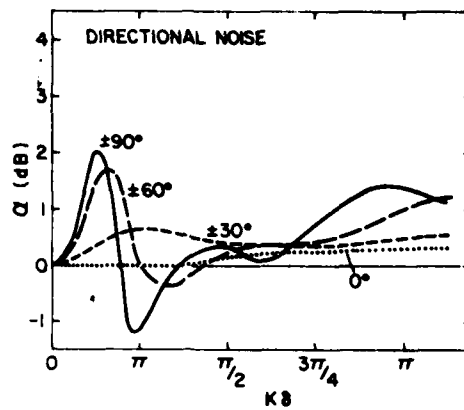
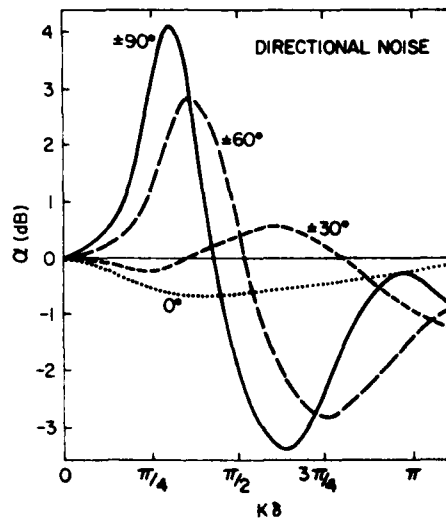13a.   Uniform sensor shading;
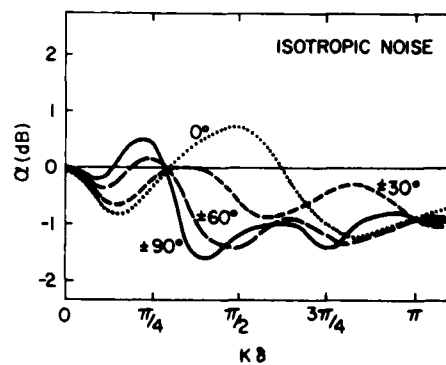
13b.   Taylor shading with first sidelobe 30 dB down.

FIG. 13.   Relative performance of the PSB and CB beamformers acting on the 5-sensor sparse array of Figure 2.   If $\alpha < 0$, the PSB is superior, and vice-versa.   Same field conditions and values of $k\delta$ and steering direction as in Figure 8.

43

14a. Uniform sensor shading;

14b. Taylor shading with first sidelobe 30 dB down.

FIG. 14. Relative performance of the PSB and CB beamformers acting on the
5-sensor sparse array of Figure 2. If $\alpha < 0$, the PSB is superior,
and vice-versa. Same field conditions and values of $k\delta$ and steering
direction as in Figure 9.

be encountered, and then calculating the variance for the given array geometry. However, the sensitivity of the variance to changes in the noise structure would make reliable variance predictions extremely difficult. Thus it appears that in the signal detection application, the PSB is probably not a practical alternative to the CB.

Finally, we consider the performance of the MVB in the signal detection application. Since the MVB provides the maximum AG possible, its suitability to this application is obvious. However, the effect of the time constraint must also be considered.

The statistics of the MVB estimate are Chi-Square distributed, but with a number of degrees of freedom less than the number available with the CB estimate, by the ratio (m-N+1)/m. N is the number of sensors in the array. For long integration times, the difference in detection indices for the CB and MVB reduces to this ratio, so that the detection thresholds differ by:

$$DT_{MVB} - DT_{CB} = 5 \log \frac{(m-N+1)}{m} . \tag{53}$$

Therefore, if the MVB detection performance is to be superior to that of the CB, its array gain must exceed the CB array gain by at least this difference.

To observe whether such differences in AG can be readily achieved, we shall examine the array gains that are obtainable under realistically modelled acoustic environments.

Plotted in Figures 15 and 16 are the array gains obtainable with the various beamformers, as a function of look direction measured from array broadside. Each figure gives the gains obtainable at two values of $k\delta$, namely $\pi/2$ and $3\pi/4$. The arrays considered in the calculations are the 10-sensor filled array and the 5-sensor minimum-redundant array of Figure 2. The acoustic fields have been modelled to be representative of the noise fields that are typically encountered in the 100-200 Hz band: 1 by a line array oriented vertically in the ocean (Figure 15), and 2 - by a line array oriented parallel to the ocean surface (Figure 16). The ambient noise field in this band of frequencies is usually dominated by noise due to distant shipping and, to a lesser degree, by noise generated at the ocean surface due to wind action[23]. We shall reference all power levels to the power of the distant shipping noise component, which has been taken from Wenz[23] as characteristic of heavy shipping conditions. Surface generated noise is chosen to be 20 dB below the shipping component, and would be typical of the noise encountered in sea state 3 conditions[23]. Expressions for the cross-spectra that would be obtained from these noise mechanisms for both vertical and horizontal sensor orientation, have been obtained from Cox[16] and Stockhausen[18]. The model of vertical directionality also includes a single plane wave arrival at -70° from array broadside, and of power 10 dB below the shipping component. For the horizontal
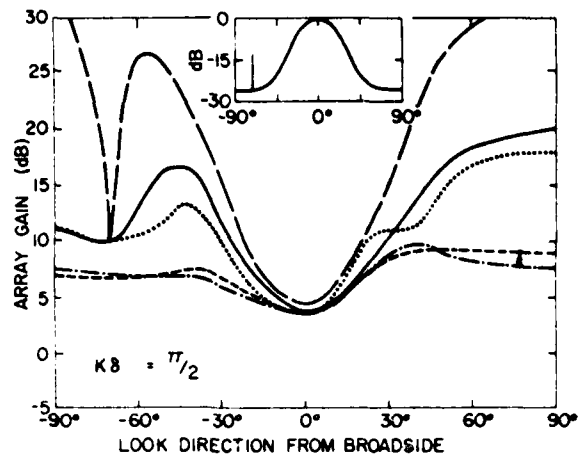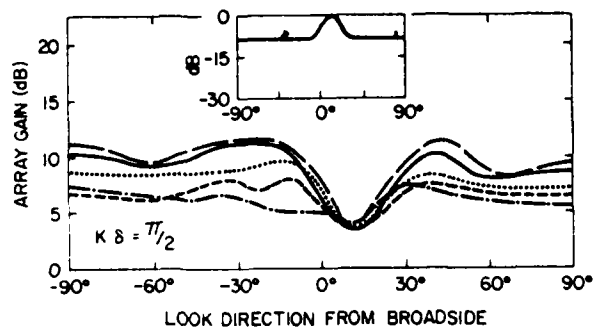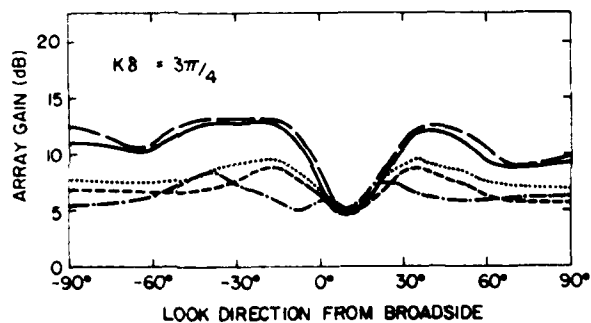
15a. $k\delta = \pi 2$;
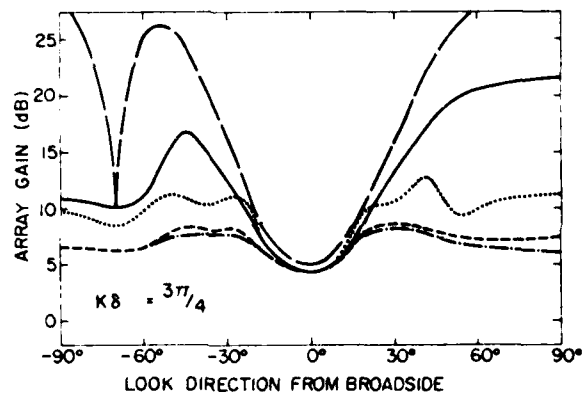
15b. $k\delta = 3\pi/4$.

FIG.15. Array gain versus look direction from array broadside, 10-sensor
filled array and 5-sensor sparse array of Figure 2. Relative noise
field directionality indicated in insert of Figure 15a. Heavy solid
line - filled array CB; long-dashed line - filled array MVB; dashed
line - sparse array CB; dot-dash line - sparse array PSB - dotted
line - sparse array MVB.

16a. $k\delta = \pi/2$

16b. $k\delta = 3\pi/4$.

FIG. 16.   Array gain versus look direction from array broadside, 10-sensor filled array and 5-sensor sparse array of Figure 2. Relative noise field directionality indicated in insert of Figure 16a. Heavy solid line - filled array CB; long-dashed line - filled array MVB; dashed line - sparse array CB; dot-dash line - sparse array PSB; dotted line - sparse array MVB.

directionality, interfering sources have been included as a plane wave arrival at (80°,-10 dB) and a source that is spread in bearing (10°,0 dB). The cross-spectra due to the last component have been modelled similarly to those due to the vertical directionality of the distant shipping noise. A spatially uncorrelated noise at 5 dB below the shipping component has also been included in the horizontal model. The models of the relative directionality are shown as inserts in each figure.

Five array gains are plotted in each figure. The solid curve displays the AG obtainable with the 10-sensor filled array CB, where the array has a uniform sensor shading. The long-dashed line is the MVB array gain for the 10-sensor filled array. The remaining three curves represent the array gain obtainable with the three beamformers, CB, PSB and MVB, each applied to the 5-sensor sparse array. In the case of the PSB, an effective array gain has been determined as equal to $AG_F - \beta$. Although the array gains of the sparse array PSB and filled array CB are equal, the former requires an increase in DT by the amount, β, in order for the beampowers to have the same detection statistics.

It is evident from Figures 15 and 16 that there is little difference in the detection performance of the CB and PSB when both beamform the sparse array. As expected, the MVB gives an array gain larger than that of the other beamformers. This is particularly true with the 10-sensor filled array and for directions away from the more directional components of the field. However, the improvement in AG for the sparse array MVB is seldom more than a few dB over that for the other sparse array beamformers. This is especially the case in Figure 16, owing to the significant spatially uncorrelated component in the field.

In order for the MVB to offer a detection performance superior to that of the other beamformers, its threshold degradation, Equation (53), must be less than the AG improvement provided by the MVB. From Figures 15 and 16, it is apparent that whether this is achieved will be dependent on a variety of parameters, such as field directionality, look direction and $k\delta$. In Figures 17 and 18 we have attempted to quantify to some degree the relative detection performance of the MVB and CB for the same array. The relative detection performance (in dB) is the difference between the MVB and CB array gains, plus the difference in detection thresholds defined by Equation (53). Whenever this quantity exceeds 0 dB, the MVB will have superior performance. The curves of Figures 17 and 18 display the relative performance as a function of the number of sensors in a filled line array. The intersensor separation, δ, is such that $k\delta = 3\pi/4$. The number of sensors varies from 1 to 30. The CB uses a uniform array shading.

Curves are grouped into three families, where each family corresponds to one of three look directions, i.e. 0°, ±45° and ±90°. For each family, the number of samples is chosen to be m = 20, 50, 100 and infinity. Note that in tactical situations, m is often ≤ 100. For m very large, the relative performance simply becomes the difference in array gains; therefore, the MVB performance will always be equal to or better than that of
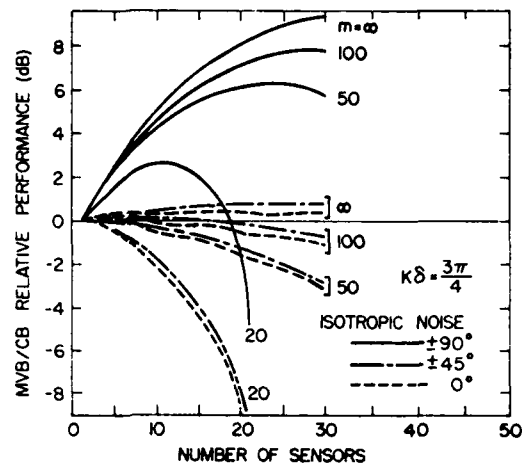
FIG. 17. Relative detection performance (in dB) of the MVB and CB versus the
number of sensors in a filled line array. $k\delta = 3\pi/4$. Number of
samples, m = 20, 50, 100 and ∞. Solid line - $\pm 90°$; dot-dash line -
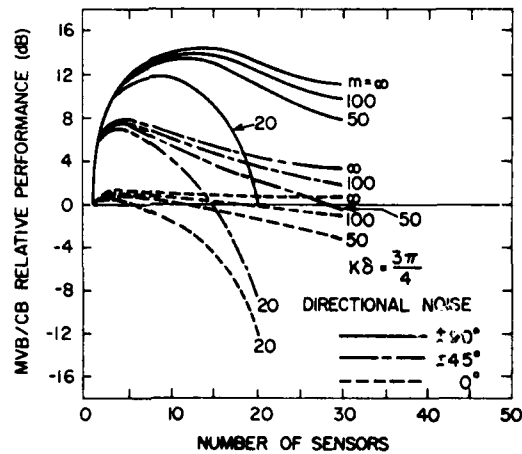$\pm 45°$; dashed line - 0°. Isotropic noise.

FIG. 18. Same as Figure 17, except using the directional noise indicated in
the insert of Figure 9a.

49

the CB. As m decreases, the order of performance may reverse. Note that the maximum number of sensors that can be used with the MVB cannot exceed m.

In Figure 17, the noise field is modelled to be isotropic. We observe that for all directions except near endfire, the CB has comparable or superior performance compared to the MVB. In Figure 18 the noise field is modelled to have the directionality indicated in the insert of Figure 9a. In this case, the MVB appears to be generally superior to the CB. Such behaviour is expected, since the MVB provides greater AG as the field becomes more directional.

As a final point of discussion, we address the question of the choice of line array geometry for use with the MVB. We shall examine the AG provided by the MVB for both the N-sensor minimum-redundant sparse array configuration and the N-sensor filled line array. The latter array is formed by reducing the aperture of the filled array from which the sparse array is formed. In Figures 19 and 20 we have plotted again the MVB array gains of Figures 15b and 16b for the 10-sensor filled array and 5-sensor minimum-redundant array. Also plotted is the MVB array gain for the 5-sensor filled array that is formed by halving the 10-sensor filled array. The latter gain is comparable to that for the sparse array for most cases. Hence, while it is difficult to be definitive based on these limited examples, it appears that the filled line array geometry is a reasonable choice if the MVB is to be used.

7. SUMMARY

This report has compared three methods of beamforming both filled and sparse line arrays, namely, the Conventional Beamformer (CB), the Principal Solution Beamformer (PSB) and the Minimum Variance Beamformer (MVB). Beamformer performance has been assessed in terms of two criteria. One is the ability of the beamformer, given no time constraint, to map the acoustic field directionality. The second criterion is the beamformer performance when the beamformer estimate of the field will be used for detection of narrowband plane wave signals. This criterion is similar to the first except in that a specified time constraint is imposed.

In examining the first criterion, we observed that provided the acoustic field was homogeneous, the sparse array PSB can return the same map of the field as the filled array CB. While the CB and PSB spatial covariance window functions may be chosen somewhat arbitrarily, the MVB window is driven by the field directionality. The MVB window function is optimum in the sense that it will minimize the influence that the acoustic power arriving from other bearings has on the beampower. Hence, the field resolution provided by the MVB will always equal or exceed that of the CB for the same array.
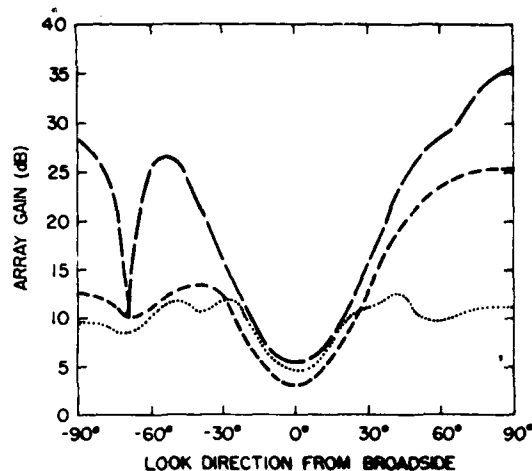
FIG. 19. MVB array gain versus look direction from array broadside. Noise
model same as for Figure 15. kδ = 3π/4. Thin solid line - 10-sensor
filled array; dotted line - 5-sensor minimum-redundant sparse array;
dashed line - 5-sensor filled array having 1/2 the aperture of the
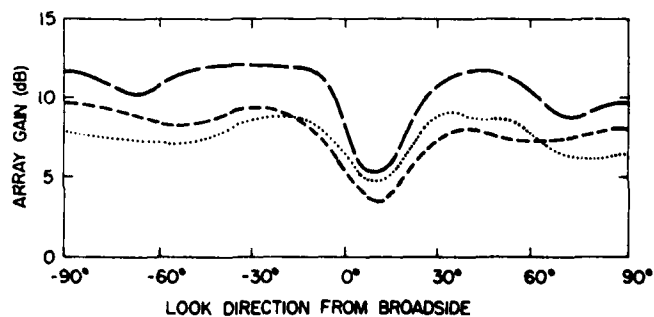10-sensor array.

FIG. 20. Same as Figure 19, except using the same noise model as for Figure 16.

51

When the field is inhomogeneous, degradation of the field mapping capability occurs for all beamformers. Both the CB and PSB exhibit apparent errors in the directions and powers of correlated plane wave signals. The PSB can also have negative powers in its map.

The MVB is seriously degraded by inhomogeneity; the MVB estimates of the powers of correlated plane wave signals are nulled by an amount dependent on the degree of their correlation and on their relative powers.

The PSB and MVB can return a map of the field directionality that may be equal to or more highly resolved than that of the CB. However, we have shown that the confidence that can be assigned to the PSB and MVB estimates obtained in a finite time interval,is often less. The relative confidence in the PSB and CB estimates is dependent on the field directionality, array geometry and frequency. However, the relative confidence in the MVB and CB estimates is dependent only on the number of sensors in the array.

The relative confidence assigned to the beamformer estimates is important when we apply the second performance criterion, where we wish to detect the presence of a narrowband plane wave signal in the beam. It was shown that the smaller confidence in the sparse array PSB estimate, compared to that of the filled array CB estimate, leads to poorer detection performance for the PSB, even though the array gains obtainable by both methods are identical. In fact, use of the PSB for beamforming the sparse array was found to have no obvious performance advantage over remaining with the CB. The MVB has one apparent advantage in the signal detection application in that it maximizes the array gain possible with the array. However, actual detection performance will also depend upon the confidence that may be placed in the MVB estimate. In general, the more directional the field, the more likely it is that the MVB will have detection performance superior to that of the CB. The more isotropic the field, the more likely it is that the reverse is true.

REFERENCES

1. G. M. Jenkins and D. G. Watts, "Spectral Analysis and Its Applications", (Holden-Day; San Francisco, 1968).

2. A. T. Moffet, "Minimum-Redundancy Linear Arrays", IEEE Trans. Antennas and Propagation AP-16, No. 2, pp. 172-175 (1965).

3. J. Leech, "On the Representation of the 1,2,....,n by Differences", J. London Math. Soc. XXXI, pp. 160-169 (1956).

4. G. W. McMahon, B. Hubley and A. Mohammed, "Design of Optimum Directional Arrays Using Linear Programming Techniques", J. Acoust. Soc. Am. 51(1), pp. 304-309 (1972).

5. R. N. Bracewell, "Radio Astronomy Techniques", in Handbuch der Physik 54, pp. 42-129 (Springer: Berlin, 1962).

6. C. R. Greene and R. C. Wood, "Sparse Array Performance", J. Acoust. Soc. Am. 63(6), pp. 1866-1872 (1978).

7. R. T. Lacoss, "Adaptive Combining of Wideband Array Data for Optimal Reception", IEEE Trans. on Geo. Sci. Elect., GE-6, pp. 78 (1968).

8. J. P. Burg, "Maximum Entropy Spectral Analysis", Ph.D. Thesis, Stanford U. (1975).

9. H. P. Bucker, "High Resolution Cross-Sensor Beamforming for a Uniform Line Array", J. Acoust. Soc. Am. 63(2), pp. 420 (1978).

10. C. A. Baird, Jr., G. G. Rassweiler, C. L. Zahm, G. P. Martin, "Adaptive Processing for Antenna Arrays", RADC-TR-72-174 (1972).

11. I. S. Reed, J. D. Mallett and L. E. Brennan, "Rapid Convergence Rate in Adaptive Arrays", IEEE Trans. on Aero. and Elect. Syst. AES-10(6), pp. 853 (1974).

12. J. Capon and N. R. Goodman, "Probability Distributions for Estimators of the Frequency-Wavenumber Spectrum", Proc. IEEE (Lett.) 58, pp. 1785 (1970).

13. J. H. Stockhausen, DREA private communication.

14. N. L. Owsley, "A Technique for Coherent Detection and Relating of Spectral Signals", NUSC-TR-5495 (1977).

15. A. Papoulis, "Probability, Random Variables, and Stochastic Processes", (McGraw-Hill: New York, 1965).

16. B. F. Cron, B. C. Hassel and F. J. Keltonic, "Comparison of Theoretical and Experimental Values of Spatial Correlation", J. Acoust. Soc. Am. 37, 523 (1965).

17. H. Cox, "Spatial Correlation in Arbitrary Noise Fields with Application to Ambient Sea Noise", J. Acoust. Soc. Am. 54(5), pp. 1289-1301 (1973).

18. J. H. Stockhausen, "Ambient Noise Vertical Directionality - A Useful Empirical Model", presented at the 90th meeting of the Acoust. Soc. Am. (Nov., 1975).

19. R. E. Collin and F. J. Zucker, "Antenna Theory Part I", (McGraw-Hill: New York, 1969).

20. Yu. A. Shreider, "The Monte Carlo Method", (Pergamon Press: Oxford, 1966).

21. R. J. Urick, "Models for the Amplitude Fluctuations of Narrow-band Signals and Noise in the Sea", J. Acoust. Soc. Am. 62(4), pp. 878 (1977).

22. R. J. Urick, "Principles of Underwater Sound" (McGraw-Hill: New York, 1967).

23. G. M. Wenz, "Acoustic Ambient Noise in the Ocean: Spectra and Sources", J. Acoust. Soc. Am. 34, pp. 1936 (1962).

DEFINITION OF "NARROWBAND"

The estimate, $\hat{\Gamma}_{rs}(f,m)$, of the cross-spectrum, $\Gamma_{rs}(f)$, at frequency, f, and for m samples is defined as:

$$\hat{\Gamma}_{rs}(f,m) = 1/m \sum_{p=1}^{m} X_{r,p}(f) X_{s,p}^{*}(f), \tag{A.1}$$

where

$$X_{r,p}(f) = 1/L \sum_{\ell=pL}^{(p+1)L-1} s_r(\ell\Delta)W(\ell)e^{-j2\pi f\Delta\ell/L} . \tag{A.2}$$

$X_{j,k}(f)$ is the result of a modified periodogram, acting on the kth segment of length L of the signal, $s_r(\ell\Delta)$, sampled at point r. Δ is the sampling period. $W(\ell)$ is the data window. The operation described by Equation (A.1) is indicated by the schematic of Figure 4.

It can be shown[1] that the expectation of $\hat{\Gamma}_{rs}(f,m)$ is:

$$\langle\hat{\Gamma}_{rs}(f,m)\rangle = \lim_{m\to\infty} \hat{\Gamma}_{rs}(f,m) = \int_{-\frac{1}{2}\Delta}^{\frac{1}{2}\Delta} \Gamma_{rs}(g)h(f-g)dg , \tag{A.3}$$

where $h(g)$ is the spectral window, and is obtained as the magnitude-squared of the Discrete Fourier Transform (DFT) of the data window, i.e.:

$$h(g) = |\sum_{\ell=0}^{L-1} W(\ell)e^{-j2\pi g\Delta\ell/L}|^2 / \sum_{\ell=0}^{L-1} |W(\ell)|^2. \tag{A.4}$$

and having normalization such that:

$$\int_{-\frac{1}{2}\Delta}^{\frac{1}{2}\Delta} h(g)dg = 1. \tag{A.5}$$

For the segment length, $T = L\Delta$, of sufficient length, i.e. for $X_{j,k}(f)$ sufficiently "narrowband", the spectral window approaches a delta function of area one. Then the cross-spectral estimator approaches being an unbiased estimator of the true cross-spectrum:

$$\langle\hat{\Gamma}_{rs}(f,m)\rangle = \lim_{m\to\infty} \hat{\Gamma}_{rs}(f,m) \sim \Gamma_{rs}(f) . \tag{A.6}$$

This qualitative definition of "narrowband" can be made quantitative by examining solutions to Equation (A.3) for specific processes. For example, assume the acoustic field consists of a single plane wave signal possessing a white, band-limited power spectrum centered at f, and of bandwidth, B_S. The cross-spectrum for such a process is:

$$\Gamma_{rs}(g) = \sigma^2/B_S \cdot e^{-j2\pi g \tau_{rs}} \qquad f-B_S/2 < g < f+B_S/2$$

$$= 0 \qquad\qquad\qquad \text{elsewhere,} \qquad\qquad (A.7)$$

where $\tau_{rs} = d_{rs}\sin\Theta_o/c$.

σ^2 is the variance, or power of the process, d_{rs} is the separation of points r and s, Θ_o is the direction of the signal relative to array broadside, and c is the speed of sound. On insertion of Equation (A.7) for $\Gamma_{rs}(g)$ in Equation (A.3), is obtained:

$$<\hat{\Gamma}_{rs}(f,m)> = \frac{\sigma^2}{B_S} e^{j2\pi f \tau_{rs}} \int_{-B_S/2}^{B_S/2} e^{-j2\pi g \tau_{rs}} h(g)\, dg . \qquad (A.8)$$

Plotted in Figure A.1 is the integral of Equation (A.8) as a function of the ratio τ_{rs}/T, for $0 \leq \tau_{rs}/T \leq 3$. This quantity should be at or near unity in order that the cross-spectral estimate be essentially an unbiased estimate of the true cross-spectrum. The spectral window used in the calculations corresponds to that for the uniform data window which, for large L, is the $Sinc^2x$ function. Curves are presented for various values of the signal bandwidth, B_S, relative to the bandwidth, $1/T$, of the DFT bin. In the limit of large B_S, the functional dependence is triangular over the range $0 \leq \tau_{rs}/T \leq 1$, since the integral of Equation (A.8) becomes the Fourier Transform of the $Sinc^2x$ function. The integral is unity at $\tau_{rs}/T = 0$, since the integral of the spectral window has been normalized to unity, according to Equation (A.5). For smaller B_S, the value at $\tau_{rs}/T = 0$ is less than unity, since the integral of the spectral window over the limited bandwidth must be less than unity. However, this value simply represents a factor by which the cross-spectral estimator can be weighted in order to remove its bias. As B_S decreases, the gradient of the curves decreases as well, and a greater value of τ_{rs}/T can be tolerated before a significant bias is introduced.

The value of bias in the estimate of the cross-spectrum that constitutes a significant bias can be assessed in terms of the error in the mean of the beamformer estimate that results because of the bias. For example, for an N-sensor filled line array of intersensor separation, δ, the mean of the CB estimate of the plane wave signal power will be $N^2\sigma^2/B_S$, if we assume that each sensor has a shading of unity. We further assume that B_S is large relative to the DFT binwidth, $1/T$, so that the dependence of the bias on τ_{rs}/T is triangular (see Figure A.1). For these assumptions,
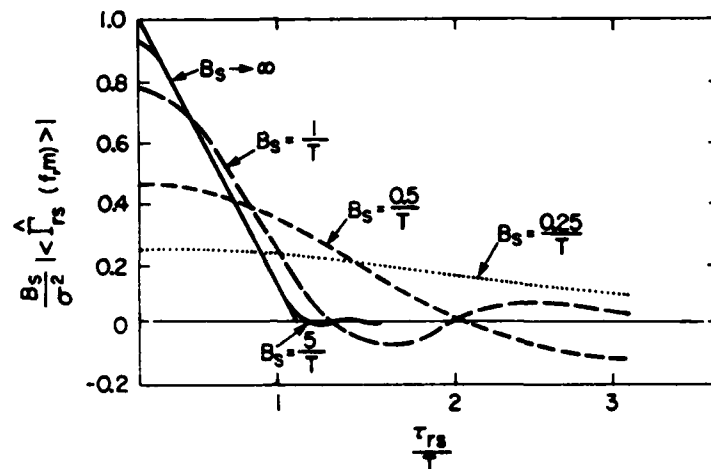
FIG. A.1 Expectation of the normalized cross-spectral estimate of a white plane wave signal of bandwidth, B_s, for $0 \leq \tau_{rs}/T \leq 3$. τ_{rs} is the plane wave propagation time between sensors r and s and T is the DFT segment length.

the mean of the CB estimate becomes approximately $\frac{N^2\sigma^2}{Bs}(1-\tau N/3T)$, where $\tau=\delta\sin\Theta_O/c$. Thus the fractional error in the beampower that is introduced by the bias in the cross-spectral estimates is $-\delta N\sin\Theta_O/3Tc$. If the array operating frequency is chosen so that the intersensor spacing, δ, is 1/2 wavelength, the error becomes $-N\sin\Theta_O/6fT$. As a numerical example of the magnitude of error that could typically occur, we choose $N=50$, $f=250$Hz, $\sin\Theta_O=1$, $T=1$ sec, and $c=5000$ ft/sec. These values yield an error of only ~0.03. However, any significant increase in the ratio, N/f, can produce a significant error unless the segment length, T, is increased proportionately. For example, if the frequency is lowered to 25 Hz and the array aperture adjusted so that the half-wavelength spacing is retained, the error in beampower becomes ~0.3. This would suggest that an increase in T to ~10 sec would be desirable.

The approximate expression, $N\sin\Theta_O/6fT$, for the beampower error allows us to establish a criterion for the use of the term "narrow-band". If the error in the beampower that we are prepared to tolerate is e, then the DFT segment length, T, must be chosen so that:

$$T > N\sin\Theta_O/6fe .\qquad\qquad(A.9)$$

For example, if $\sin\Theta_O=1$ and $e=0.05$, then T must be $> 3N/f$. Then if N is 50 and f is 250 Hz, the segment length must exceed 0.6 sec.

APPENDIX B

VARIANCE OF THE PSB ESTIMATE

The sparse array PSB estimate of the field directionality at frequency, f, and at bearing, Θ_0, to array broadside, was defined in Equation (25) to be:

$$\hat{P}_{PSB}(f,\Theta_0,m) = \sum_{n=-(N-1)}^{N-1} u_s(n)e^{-jnk\delta\sin\Theta_0}\,\Theta_s(f,m,n), \qquad (B.1)$$

where:
$$\Theta_s(f,m,n) = \sum_{i=1}^{N-n} \hat{\Gamma}_{i+n,i}(f,m)\epsilon_i\epsilon_{i+n} \qquad n \geq 0 ,$$

$$= \Theta_s^*(f,m,-n), \qquad n < 0 ,$$

and the corresponding filled array has N sensors of intersensor spacing, δ. $\epsilon_j=0$ or 1, depending on the absence or presence in the sparse array of the jth filled array sensor. The $u_s(n)$ is the spatial covariance window for the spacing, $n\delta$. $\hat{\Gamma}_{rs}(f,m)$ is the m-sample cross-spectral estimate for sensors r and s, and is given by Equation (A.1).

The variance, $\sigma^2_{PSB}(f,\Theta_0,m)$, of the PSB estimate will be:

$$\sigma^2_{PSB}(f,\Theta_0,m) = \sigma^2_{PSB}(f,\Theta_0,1)/m , \qquad (B.2a)$$

$$= \frac{<\hat{P}_{PSB}(f,\Theta_0,1)^2> - <\hat{P}_{PSB}(f,\Theta_0)>^2}{m} , \qquad (B.2b)$$

where $<\cdot>$ indicates expectation. Equation (B.2a) results since the PSB estimate for m samples can be expressed as the average of m PSB estimates for 1 sample. Therefore, we shall first calculate $\sigma^2_{PSB}(f,\Theta_0,1)$, and then apply Equation (B.2a) to obtain $\sigma^2_{PSB}(f,\Theta_0,m)$.

We shall assume that the acoustic field is stationary and homogeneous, and that the output of each DFT bin is a zero-mean, narrowband complex Gaussian process. If the process is sufficiently narrowband, then the cross-spectral estimate is an unbiased estimate of the true cross-spectrum, i.e. $<\hat{\Gamma}_{rs}(f,m)>\sim\Gamma_{rs}(f)$. To calculate the variance, we require one more expectation, namely:

$$<\hat{\Gamma}_{ij}(f,1)\hat{\Gamma}_{k\ell}(f,1)> = <X_{i,p}(f)X_{j,p}^*(f)X_{k,p}(f)X_{\ell,p}^*(f)> \qquad (B.3a)$$

$$= <\hat{\Gamma}_{ij}(f,1)><\hat{\Gamma}_{k\ell}(f,1)>+<\hat{\Gamma}_{i\ell}(f,1)><\hat{\Gamma}_{kj}(f,1)>$$

$$\sim \Gamma_{ij}(f)\Gamma_{k\ell}(f)+\Gamma_{i\ell}(f)\Gamma_{kj}(f) \qquad (B.3b)$$

where Equation (B.3a) holds if the $X_{i,p}(f)$ are complex Gaussian variates.

For the above assumptions, we obtain for the variance, Equation (B.2):

$$\sigma^2_{PSB}(f,\Theta_0,m) = \frac{1}{m} \left[|u_s(0)|^2 A_{00} + 2Re \sum_{p=1}^{N-1} \sum_{q=1}^{N-1} u_s^*(p) u_s(q) (A_{pq}e^{-j(p+q)\eta} + B_{pq}e^{-j(p-q)\eta}) \right.$$

$$\left. + 4Re \sum_{p=1}^{N} \sum_{q=1}^{N-1} u_s(0) u_s(q) C_{pq}e^{-jq\eta} \right]$$

where: $\eta = k\delta\sin\Theta_0$

and

$$A_{pq} = \sum_{i=1}^{N-p} \sum_{j=1}^{N-q} \epsilon_i \epsilon_j \epsilon_{i+p} \epsilon_{j+q} \Gamma_{j+q-i}(f) \Gamma_{i+p-j}(f) \quad ,$$

$$B_{pq} = \sum_{i=1}^{N-p} \sum_{j=1}^{N-q} \epsilon_i \epsilon_j \epsilon_{i+p} \epsilon_{j+q} \Gamma_{i-j}(f) \Gamma_{j+q-i-p}(f) \quad ,$$

$$C_{pq} = \sum_{j=1}^{N-q} \epsilon_p \epsilon_j \epsilon_{j+q} \Gamma_{p-j}(f) \Gamma_{j+q-p}(f) \quad .$$

$\Gamma_n(f) = \Gamma_{-n}^*(f)$, and is the cross-spectrum for all pairs of sensors having separation, $n\delta$.

We examine the special case where all $\epsilon_i = 1$, i.e. the array is filled, and choose the window function, $u_s(n)$ to be the rectangular window. After some tedious algebra, one can show that the variance reduces to:

$$\sigma^2_{PSB}(f,\Theta_0,m) = \frac{<\hat{P}_{CB}(f,\Theta_0)>^2}{m} . \qquad (B.6)$$

$<P_{CB}(f,\Theta_0)>$ is the expectation of the filled array CB estimate, as defined by Equation (15), where the sensor shading is uniform. This result is expected since for the above choice of windows, the filled array CB and PSB estimates have an identical formulation. Since the CB estimate has been shown to be a Chi-Square variate, the relationship between the mean and variance must take the form of Equation (B.6).

APPENDIX C

MONTE CARLO TECHNIQUES

With the availability of high-speed computers, Monte Carlo tech-
niques have become a useful tool for estimating the properties of any pro-
cess which requires a statistical description. The principle is that by
repeated passing of random variates of assumed statistics through a
numerical simulation of an operator, the statistics at the output of the
operator may be estimated.

One important application of Monte Carlo techniques lies in the
determination of the probability density function of the output of an
operator having a stochastic process as its input. As a specific example
of this application, we require knowledge of the density function which
describes the statistics of the PSB estimate of the acoustic field direc-
tionality, according to Equation (25). We assume that the field is
stationary and homogeneous, and that the sensor outputs in any DFT bin will
be zero-mean narrowband complex Gaussian processes. The development of the
Monte Carlo technique will proceed as follows. First, the outputs in the
DFT bin at frequency, f, for the N array sensors are simulated by generation
of N independent zero-mean complex Gaussian variates, each having a variance
of unity. These N complex variates are then transformed into N correlated
complex Gaussian variates which exhibit the cross-spectral properties of
the acoustic field which is being modelled. An estimate of the cross-
spectral matrix for one sample is produced from these variates, and
inserted in the beamformer operator, Equation (25), to obtain one estimate
of the beampower. The procedure is repeated a large number of times to
build up the probability density function of the beampower estimate.

The major weakness in the technique is that while adequate
statistical confidence can be obtained over the central portion of the
density function, an unrealistically large number of trials can be required
to predict the function far into its tails.

The density function obtained by the method described above
represents the power statistics for a single sample, $m=1$. For $m > 1$, there
are two methods of estimating the appropriate function. In one method,
the density function for one sample must be convolved with itself accord-
ing to the number of averages wanted. Such repeated convolutions will
quickly remove the small statistical fluctuations in the density function
that are inherent in the Monte Carlo technique. In the second method, m
estimates of the cross-spectral matrix are obtained prior to application of
the beamformer operator. This method will require m times the number of
random numbers to be generated as in the first method.

DOCUMENT CONTROL DATA - R & D

(Security classification of title, body of abstract and indexing annotation must be entered when the overall document is classified)

1. ORIGINATING ACTIVITY	2a. DOCUMENT SECURITY CLASSIFICATION
	UNCLASSIFIED
	2b. GROUP AD - AC 72 367

3. DOCUMENT TITLE

A STUDY OF FILLED AND SPARSE LINE ARRAY BEAMFORMERS

4. DESCRIPTIVE NOTES (Type of report and inclusive dates)

5. AUTHOR(S) (Last name, first name, middle initial)

R. S. WALKER

6. DOCUMENT DATE	7a. TOTAL NO. OF PAGES	7b. NO. OF REFS
SEPTEMBER 1980	67	23

8a. PROJECT OR GRANT NO.	9a. ORIGINATOR'S DOCUMENT NUMBER(S)
	DREA Technical Memorandum 80/G
8b. CONTRACT NO.	9b. OTHER DOCUMENT NO.(S) (Any other numbers that may be assigned this document)

10. DISTRIBUTION STATEMENT

11. SUPPLEMENTARY NOTES | 12. SPONSORING ACTIVITY

13. ABSTRACT   The paper considers various methods of frequency-domain beamforming for a line array of hydrophones. The line array geometries are restricted to uniform sensor spacings (i.e. filled array) or a geometry in which sensors are eliminated from the filled structure (sparse array). The methods to be examined include the conventional phase-to-plane beamformer (CB), the data-adaptive Minimum Variance beamformer (MVB), and the Principal-Solution beamformer (PSB). The beamformer performance is assessed on the basis of two criteria. The first is the ability of the beamformer to map the directionality of the acoustic field. The integration time used in producing the map is unrestricted: hence, only first-order beamformer statistics influence the performance. The second criterion is the ability to detect narrowband, directional signals against the noise. Here the integration time is finite, and higher-order beamformer statistics become important. We shall show that the PSB has advantages over the CB for mapping of the directionality. However, no advantage exists in the signal detection application. The MVB provides the directionality map that is least influenced by leakage. However, its detection performance is superior to that of the CB only if the noise field is highly directional.

DSIS
70-241

KEY WORDS

- underwater acoustics
- passive sonar
- filled line array
- sparse line array
- beamformer
- directionality
- signal detection
- confidence intervals
- inhomogeneity
- Monte Carlo
- computer simulation
- cross-spectral matrix

INSTRUCTIONS

1. ORIGINATING ACTIVITY: Enter the name and address of the organization issuing the document.

2a. DOCUMENT SECURITY CLASSIFICATION: Enter the overall security classification of the document including special warning terms whenever applicable.

2b. GROUP: Enter security reclassification group number. The three groups are defined in Appendix 'M' of the DRB Security Regulations.

3. DOCUMENT TITLE: Enter the complete document title in all capital letters. Titles in all cases should be unclassified. If a sufficiently descriptive title cannot be selected without classification, show title classification with the usual one-capital-letter abbreviation in parentheses immediately following the title.

4. DESCRIPTIVE NOTES: Enter the category of document, e.g. technical report, technical note or technical letter. If appropriate, enter the type of document, e.g. interim, progress, summary, annual or final. Give the inclusive dates when a specific reporting period is covered.

5. AUTHOR(S): Enter the name(s) of author(s) as shown on or in the document. Enter last name, first name, middle initial. If military, show rank. The name of the principal author is an absolute minimum requirement.

6. DOCUMENT DATE: Enter the date (month, year) of Establishment approval for publication of the document.

7a. TOTAL NUMBER OF PAGES: The total page count should follow normal pagination procedures, i.e., enter the number of pages containing information.

7b. NUMBER OF REFERENCES: Enter the total number of references cited in the document.

8a. PROJECT OR GRANT NUMBER: If appropriate, enter the applicable research and development project or grant number under which the document was written.

8b. CONTRACT NUMBER: If appropriate, enter the applicable number under which the document was written.

9a. ORIGINATOR'S DOCUMENT NUMBER(S): Enter the official document number by which the document will be identified and controlled by the originating activity. This number must be unique to this document.

9b. OTHER DOCUMENT NUMBER(S): If the document has been assigned any other document numbers (either by the originator or by the sponsor), also enter this number(s).

10. DISTRIBUTION STATEMENT: Enter any limitations on further dissemination of the document, other than those imposed by security classification, using standard statements such as:

    (1) "Qualified requesters may obtain copies of this document from their defence documentation center."

    (2) "Announcement and dissemination of this document is not authorized without prior approval from originating activity."

11. SUPPLEMENTARY NOTES: Use for additional explanatory notes.

12. SPONSORING ACTIVITY: Enter the name of the departmental project office or laboratory sponsoring the research and development. Include address.

13. ABSTRACT: Enter an abstract giving a brief and factual summary of the document, even though it may also appear elsewhere in the body of the document itself. It is highly desirable that the abstract of classified documents be unclassified. Each paragraph of the abstract shall end with an indication of the security classification of the information in the paragraph (unless the document itself is unclassified) represented as (TS), (S), (C), (R), or (U).

The length of the abstract should be limited to 20 single-spaced standard typewritten lines; 7½ inches long.

14. KEY WORDS: Key words are technically meaningful terms or short phrases that characterize a document and could be helpful in cataloging the document. Key words should be selected so that no security classification is required. Identifiers, such as equipment model designation, trade name, military project code name, geographic location, may be used as key words but will be followed by an indication of technical context.

DATE
ILMED

—8